JOURNAL OF GEOPHYSICAL RESEARCH, VOL. ???, NO. , PAGES 1–41,

# Neogene Overflow of Northern Component Water at the Greenland-Scotland Ridge

**H.R. Poore,[1] R. Samworth,[2] N.J. White,[1] S.M. Jones,[3] I.N. McCave,[1]**

H.R. Poore, Dept. of Earth Sciences, University of Cambridge Downing Street, Cambridge. CB2 3EQ. poore@esc.cam.ac.uk

[1]Dept. of Earth Sciences, University of Cambridge, Downing Street, Cambridge. CB2 3EQ.

[2]Statistical Laboratory, Centre for Mathematical Studies, University of Cambridge, Wilberforce Road, Cambridge. CB3 0WB.

[3]S.M. Jones, Dept. of Geology, Trinity College, University of Dublin, Dublin 2, Ireland

**Abstract.** In the North Atlantic Ocean, flow of North Atlantic Deep Water (NADW), and its ancient counterpart Northern Component Water (NCW), across the Greenland-Scotland Ridge (GSR) are thought to have played an important role in ocean circulation. Over the last 60 Ma, the Iceland Plume has dynamically supported an area which encompasses the GSR. Consequently, bathymetry of the GSR has varied with time due to a combination of lithospheric plate cooling and fluctuations in the temperature and buoyancy within the underlying convecting mantle. Here, we reassess the importance of plate cooling and convective control on this northern gateway for NCW flow during the Neogene period, following *Wright and Miller* [1996]. To tackle the problem, benthic foraminiferal isotope datasets have been assembled to examine $\delta^{13}$C gradients between the three major deep water-masses (i.e. Northern Component Water, Southern Ocean Water and Pacific Ocean Water). Composite records are reported on an astronomical time scale and a non-parametric curve-fitting technique is used to produce regional estimates of $\delta^{13}$C for each water mass. Confidence bands were calculated and error propagation techniques used to estimate %NCW and its uncertainty. Despite obvious reservations about using long-term variations of $\delta^{13}$C from disparate analyses and settings, and despite considerable uncertainties in our understanding of ancient oceanic transport pathways, the variation of NCW through time is consistent with independent estimates of the temporal variation of dynamical support associated with the Iceland Plume. Prior to 12 Ma, $\delta^{13}$C patterns overlap and %NCW cannot be isolated. Significant long-period variations are evident, which are consistent with previously published work. From 12 Ma, when lithospheric cooling probably caused the GSR to submerge completely, long-period $\delta^{13}$C patterns diverge significantly and allow reasonable %NCW estimates to be made. Our most robust result is a dramatic increase in NCW overflow between 6 and 2 Ma when dynamical support generated by the Iceland Plume was weakest. Between 6 and 12 Ma, a series of variations in NCW overflow have been resolved.

## 1. Introduction

*Wright and Miller* [1996] argue that there is a strong negative correlation between the percentage of Northern Component Water (%NCW), which affects $\delta^{13}$C values in the Southern Ocean, and vertical motions of the Greenland-Scotland Ridge (GSR) during Neogene times (Figures 1–3). These vertical motions occur with at least two time scales. First, long-term subsidence of the GSR (time scale of 10s of millions of years) is controlled by cooling of the lithospheric plate as it drifts away from the mid-oceanic ridge. Secondly, short-term uplift and subsidence excursions (time scale of 1–10 Ma) are controlled by rapid buoyancy fluctuations within the Iceland Plume. This plume is a major convective upwelling within the mantle which has had an important effect upon the structural development of the North Atlantic Ocean over the last 60 Ma.

Such changes in elevation of the GSR could affect flux of NCW into the Southern and Pacific Oceans. When the GSR is deeper (i.e. the Iceland Plume is cooler) a larger volume of deep water can flow over the ridge, thus increasing %NCW present in the Southern Ocean (Figure 3). When the Iceland Plume is hotter and the GSR is shallower, production of NCW could be significantly reduced. This lock-gate mechanism is important because it might help to improve our understanding of temporal changes within the Iceland Plume and thus contribute to knowledge of the dynamics of mantle convection. It may also help to gauge the strength of thermohaline circulation and hence the influence of variations in NCW production on Neogene climate.

Present-day NCW (i.e. North Atlantic Deep Water, NADW) has three principal sources (Figure 1): (i) overspill from the Norwegian-Greenland Seas through the Faroe-Shetland Channel (1.7 Sv); (ii) overspill through the Denmark Straits (2.9 Sv); and (iii) convective overturning within the Labrador Sea [*Dickson and Brown*, 1994]. It remains unclear when the Labrador Sea became an important source of deep water [*Mikolajewicz and Crowley*, 1997; *Burton et al.*, 1997; *Lear et al.*, 2003]. Roughly 40% of the total NADW flux is sourced from the Labrador Sea [*Schmitz Jr. and McCartney*, 1993]. We assume that if

the cold deep core of NADW from the Faroe-Shetland Channel and from the Denmark Straits is reduced significantly, then a large reduction in %NCW in the Southern Ocean results because the cold deep core of NADW consists primarily of GSR overflow water and not of warmer, less salty Labrador Sea Water.

At present, flow of cold, deep NCW from the Norwegian-Greenland Sea into the North Atlantic Ocean is impeded by the GSR, which extends east and west from Iceland (Figure 1b). The present-day depth of the deeper channels through this ridge is no greater than ∼850 m and allows a total of 5.6 Sv ($10^6$ $m^3$) of deep water to flow over the barrier [*Dickson and Brown*, 1994], although its volume increases by entrainment downstream of channel exits. Hence Norwegian Sea Overflow Water (NSOW) forms much of the Lower North Atlantic Deep Water (LNADW). At present, the core of NSOW flows at depths of 500–600 m, descending as it travels southward through the Faroe-Bank Channel [*Kuijpers et al.*, 2002]. Cold northern waters are restricted to ∼150 m above the sea bed in this deepest gateway (Figure 1b). Therefore GSR overflow waters should be sensitive to plume-related dynamic uplift.

Over the last 10 years, much new benthic foraminiferal $\delta^{13}C$ (and $\delta^{18}O$) data have become available. These new data have an average sample interval of up to ∼5 ka and facilitate improved core-to-core correlation [*Billups et al.*, 2004, Figures 4 and 5]. North Atlantic records include data from ODP Site 925 (*Billups et al.* [1997, 1998] and H. Pfuhl, written communication, 2004). Pacific Ocean records include analyses from ODP Site 846 (0–7.4 Ma, *Mix and Shackleton* [1995]; *Shackleton et al.* [1995b]). Most of the Southern Ocean data is from ODP Legs 177 and 185. The geological time scale has also undergone revision thanks to the availability of astronomically tuned records for the Neogene period [*Lourens et al.*, 2004]. With a greatly improved database and timescale, we can more accurately construct end-member records of carbon isotopes. Finally, we present a new strategy for fitting $\delta^{13}C$ records with smooth functions and confidence bands. In this way,

we can estimate the variation of NCW overflow and its associated uncertainty through time and revisit the *Wright and Miller* [1996] hypothesis.

## 2. Benthic Carbon Isotope Datasets

A range of proxies is used to understand paleocirculation patterns, including $\delta^{13}$C and trace metals (e.g. Neodymium, Cadmium). Following *Wright and Miller* [1996], we exploit $\delta^{13}$C because samples can be easily assigned ages, records are of sufficiently high resolution, and there is now a wealth of published and unpublished analyses. $\delta^{13}$C is a useful tracer of water masses because it reflects the nutrient content of deep water [*Ruddiman*, 2001], although care must be taken in choosing species that accurately record the isotopic composition of seawater. North Atlantic Deep Water is $^{13}$C rich because surface waters from which it forms have previously been depleted in both nutrients and $^{12}$C (manifested by a decrease of 1 ‰) within the subtropical Atlantic Ocean. In contrast, deep water formed in the Weddell Sea contains more nutrients and less $^{13}$C because surface waters sink without being reventilated. $\delta^{13}$C is not a conservative tracer. However, given a residence time of deep water in the deep Atlantic of $\leq$300 yrs [*Broecker and Peng*, 1982], it is reasonable to model benthic $\delta^{13}$C as a conservative tracer. Benthic $\delta^{13}$C can then be used to quantify the mixing of two water masses at a particular site [*Kroopnick*, 1985; *Oppo and Fairbanks*, 1987]. One minor complication in understanding benthic $\delta^{13}$C gradients is the existence of the 'Mackensen effect' [*Mackensen et al.*, 1993], which can lead to extremely low $\delta^{13}$C values. However, this effect is probably smaller than the ventilation effect and as far as is possible we use epibenthic foraminifera such as *Cibicidoides wuellerstorfi*, which should circumvent this problem.

**2.0.1. Benthic $\delta^{13}$C end-members.** Benthic stable isotope data have been compiled from sediment cores located in the North Atlantic Ocean, in the Atlantic sector of the Southern Ocean and in the Pacific Ocean (Figure 4 and 5). Each region acts as an end-member in the mixing equation of *Oppo and Fairbanks* [1987] which is used to find

an estimate of the percentage overflow of NCW through time. The estimate of %NCW, $\widehat{\text{NCW}}$, is given by

$$\widehat{\text{NCW}} = \frac{\delta^{13}\text{C}_{SO} - \delta^{13}\text{C}_{PO}}{\delta^{13}\text{C}_{NA} - \delta^{13}\text{C}_{PO}} \times 100, \quad (1)$$

where $\delta^{13}\text{C}_{SO}$, $\delta^{13}\text{C}_{PO}$ and $\delta^{13}\text{C}_{NA}$ are estimates of $\delta^{13}$C for the Southern, Pacific, and North Atlantic Oceans. Note that in the text, we refer to %NCW rather than its estimate.

It is important to choose the geographical location of each dataset carefully so that the true variation of each end-member is reflected in the composite record. North Atlantic records are taken from sites which are sufficiently far north and from depths at which benthic foraminifera are likely to be fully bathed by the North Atlantic end-member. Southern Ocean sites should ideally be located beneath the mixing zone of Upper Circumpolar Deep Water (UCDW) and NCW, a boundary that we assume remains fixed through time. This mixing zone is likely to have changed both its geographical position and its depth, but we lack data to constrain any movement during Neogene times. Pacific Ocean sites should reflect Pacific Ocean deep water and therefore should not include records from restricted sub-basins such as ODP Site 677 [*Mix and Shackleton*, 1995; *Oppo et al.*, 1995]. The Pacific Ocean can exhibit east-west $\delta^{13}$C gradients which result from non-conservative $\delta^{13}$C effects (i.e. water-mass aging caused by accumulation of nutrients; *Kroopnick* [1985]). Pacific $\delta^{13}$C gradients are problematic but difficult to circumvent, given the geographical distribution of reliable Neogene high-resolution data [*Whitman and Berger*, 1993].

Sources of data used for each oceanic end-member are given in Figure 5 and in Tables 1–3. $\delta^{13}$C data are quoted to the PDB standard and species disequilibria are corrected using the species offsets of *Graham et al.* [1981]; *Shackleton and Hall* [1984]; *Müller et al.* [1991] and *Katz et al.* [2003]. Where multiple samples are used or where individual data points are obviously outliers, $\delta^{13}$C values obtained from more unreliable species have been removed [*Katz et al.*, 2003]. We have also removed data points for which both carbon and oxygen isotopes were greater than two estimated standard deviations from the regression

curve. We subsequently refitted the data using our local linear kernel regression procedure. The distribution of standard deviations then better approximated a normal distribution, which is an assumption made during the fitting procedure.

Records used to construct Atlantic and Pacific end-members are mostly similar to those used by *Wright and Miller* [1996]. Our North Atlantic composite record now includes ODP Site 925 for part of the late Miocene and Early Pliocene (6.240–3.281 Ma). *Billups et al.* [1998] have shown that Site 925, at 3042 m mostly reflects NCDW which is dominant to depths of 3000 m on Ceara Rise during the Early Pliocene. Despite its southerly location we therefore think that Site 925 adequately records the variation in $\delta^{13}$C of NCW. In constructing the Pacific end-member, we have also replaced ODP Site 677 with ODP Site 846 and have supplemented DSDP Site 289 with data from DSDP Sites 296, 574A and ODP Sites 806, 846. Our most significant revision concerns the Southern Ocean end-member. Recent ODP cruises have recovered sediment cores which span the age interval of interest and which lie beneath the modern mixing zone of CDW and NADW [*Billups*, 2002]. New material from Leg 177 Sites 1088 [*Billups*, 2002], and 1090 [*Billups et al.*, 2002, 2004] provide an opportunity to re-examine the Southern Ocean composite $\delta^{13}$C record in detail.

**2.0.2. Age models.** Accurate dating of compiled records is a major concern in order to ensure that $\delta^{13}$C gradients can be reliably interpreted. Astronomical dating of magnetobiostratigraphic datums significantly improves the correlation of different records. $\delta^{13}$C records from each site were placed on the astronomically calibrated time scale of *Lourens et al.* [2004] by linearly interpolating between magnetobiostratigraphic datums (Figure 5). Age models for the different benthic $\delta^{18}$O records were then adjusted by comparison with an astronomically tuned $\delta^{18}$O record in order to refine correlation of the three oceanic end-members (Figure 6). A composite isotope sequence from V19–30, ODP 677 and ODP 846 was used for the 0–6 Ma interval (http://delphi.esc.cam.ac.uk, [*Shackleton and Pisias*, 1985; *Shackleton et al.*, 1990, 1995b, a]). Data from ODP Site 982 [*Hodell et al.*, 2001]

were used between 6 and 9 Ma. A sequence from ODP Site 926 was used for the 14–16 Ma interval (N.J. Shackleton, written communication 2004) and data from ODP Site 1090 were used to calibrate the rest of the Neogene reference $\delta^{18}$O record [*Billups et al.*, 2004]. The 9–14 Ma interval does not have high resolution benthic $\delta^{18}$O records from sites which have been astronomically tuned. Instead, a combination of Leg 154 magnetic susceptibility and reflectance data together with $\delta^{18}$O records from sites 704 and 747, which have reliable magnetostratigraphy and continuous sedimentation, were used as reference sequences to which other datasets could be correlated. The age model for 9–14 Ma does have large uncertainties compared with data outside this range but the $\delta^{13}$C records are sparse, so correlation to future astronomically tuned benthic oxygen data is unlikely to alter the age models significantly. When depth-age constraints were added to the overall age model, resulting sedimentation rates were checked to ensure that sedimentation rates varied smoothly except at known hiatuses and unconformities.

**2.0.3. Spectral analysis.** Spectral analysis of the corresponding benthic oxygen isotope data provides an useful check on the quality of age models applied to the carbon isotope data. The oxygen isotopic composition of sea water primarily reflects global ice volume [*Imbrie et al.*, 1984], which responds to changes in the seasonal input of insolation at different latitudes. These changes are controlled by three orbital parameters of the earth: eccentricity (100 and 400 ka periods), obliquity (41 ka) and precession (19 and 23 ka).

Both Southern and Pacific Oceans show that significant orbital frequencies are present, mostly as a result of the inclusion of astronomically tuned datasets. All oxygen data are coherent with the calculated insolation curve for higher orbital periodicities in both these oceans. Precession frequencies are only weakly coherent (below 80% significance level) suggesting that data are poorly tuned at these periodicities. This weakness is unsurprising given the *caveats* mentioned above, the temporal range of the data, and the coarser sampling intervals for the Miocene epoch compared with Plio-Pleistocene times.

North Atlantic composite records have the weakest periodicities with peaks in power which are barely significant compared with background noise.

## 3. Statistical Analysis

There are significant errors in $\delta^{13}$C measurements and in their ages, both of which propagate through the differences in Equation 1 to affect our estimate of %NCW. The source of error in $\delta^{13}$C is both measurement error, whose standard deviation ranges between 0.05 and 0.1‰, and in vital effect species correction factors, which *Graham et al.* [1981] quote as ranging between 0.12 and 0.46‰. In order to calculate the variation of %NCW with time, each composite $\delta^{13}$C record is first fitted with a smooth function. There are numerous ways in which this fitting can be carried out. Here, we outline an approach which has two important features. First, we allow the bandwidth of the kernel estimator to vary through time. This flexibility ensures that large variations in sample distribution are accommodated. Secondly, confidence bands for best-fitting functions are constructed. We give a brief discussion of the techniques used and refer the interested reader to *Samworth and Poore* [2005] for further details.

### 3.1. Local Linear Kernel Regression

Our first task is to fit a smooth curve through each composite record. Gaussian filters are often used for this purpose [e.g. *Mix and Shackleton*, 1995; *Wright and Miller*, 1996; *Zachos et al.*, 2001]. In the statistical literature, this locally weighted mean would be referred to as a local constant kernel estimator with a Gaussian kernel or weight function. The more sophisticated local linear kernel estimator, however, has the advantage of significantly reduced bias, particularly at the boundaries of the data, or in regions of high sample resolution [*Fan and Gijbels*, 1996]. The local linear estimator for $(x_i, y_i)$ pairs is given by

$$\hat{m}_h(x) = \frac{1}{n}\sum_{i=1}^{n} \frac{\{s_2 - s_1(x_i - x)\}K_h(x_i - x)}{s_2 s_0 - s_1^2}\, y_i \qquad (2)$$

where

$$s_r = \frac{1}{n}\sum_{i=1}^{n}(x_i - x)^r K_h(x_i - x), \quad r = 0, 1, 2,$$

and the scaled kernel, $K_h(\cdot) = h^{-1}K(\cdot/h)$, satisfies $\int K_h = 1$.

For both local constant and local linear estimators, the crucial choice is that of the bandwidth, $h$, which controls the amount of smoothing: too small a value of $h$ results in a spikey, undersmoothed curve; equally if $h$ is too large then the data are oversmoothed leading to a loss of the signal.

Oceanographic records are generally fitted using a Gaussian filter with a constant bandwidth. The main difficulty with this approach is that data distribution is inevitably highly non-uniform as a consequence of records being pooled from different cores, sampled at different resolutions, and because of gaps and unconformities. A bandwidth which is appropriate in a region of high resolution data may be many times smaller than that in a region of sparse data. We have sidestepped this issue by dividing the age range into blocks of approximately equal sample resolution; we then chose a separate bandwidth for each block. Since we are less interested in the rate of change of $\delta^{13}$C, continuity of first and second derivatives is not of primary concern. Pacific, Southern and North Atlantic composite records were divided into 21, 16 and 12 blocks, respectively, and appropriate bandwidths were chosen for each block. Our regression method slides the chosen kernel through the age range of the composite record. At boundaries of blocks, part of the kernel cannot be used to weight $(x_i, y_i)$ pairs, which results in a large bias. To reduce this effect, we take the half-width of the kernel and extend the age range of each block by this width.

### 3.2. The SIMEX Algorithm

In addition to the error in the $y$-direction associated with measuring $\delta^{13}$C level at a given age, there is also an error in the $x$-direction associated with assigning an age to a particular sample. This error arises from several sources, including the assumption of a constant sedimentation rate between age-depth control points and the fact that the ages

and composite depths of these control points are not precisely known. Temporal errors have often been ignored in previous studies. However, errors-in-variables techniques have been developed in statistical analysis for handling this problem.

We have applied the Simulation Extrapolation (SIMEX) algorithm of *Cook and Stefanski* [1994] and *Carroll et al.* [1995] to all data. The results for the first block of the Pacific Ocean record are shown in Figure 7. The SIMEX algorithm analyses the effect of adding additional noise of known standard deviation to the age of each point and it then extrapolates backwards to estimate the effect of having no noise at all. Addition of this extra noise tends to blur peaks and troughs in the estimated curve. The final SIMEX estimate helps to clarify these features.

### 3.2.1. Confidence bands.

We have calculated 95% confidence bands for each block in order to estimate uncertainties of each composite $\delta^{13}$C record. Each confidence band is interpreted as a region which contains the true (i.e. unobserved) $\delta^{13}$C variation over the age range of the block in question with a probability of 0.95. Many techniques for the construction of confidence bands in nonparametric regression problems have been published in the statistical literature. We looked in detail at those proposed by *Xia* [1998] and at two constructions proposed by *Claeskens and van Keilegom* [2003]. We prefer the *Xia* [1998] confidence bands which are generally wider than those of the first construction of *Claeskens and van Keilegom* [2003]. Their second construction was found to be very sensitive to small changes in bandwidth for our data. The *Xia* [1998] bands behave in a more robust and conservative way which is suitable for our purposes (Figure 8). These bands also allow bias of the regression estimate at peaks and troughs to be estimated so that bands are not simply centered around the regression estimate. Unfortunately, there is currently no theoretical support for calculating confidence bands around SIMEX estimates. Therefore, we only calculate Xia bands around the bias-corrected local linear regression estimate.

Confidence bands for blocks with small amounts of data (usually blocks with a small age range) must be treated with caution because of undercoverage problems. In other words, the probability that a confidence band contains the true regression curve may be less than 95% if there is a limited amount of data (i.e. $\leq$50 data points per block). Intervals that may be particularly susceptible to this problem lie between 6 and 7 Ma, and 12.5 and 13.5 Ma in the Pacific Ocean.

## 4. End-Member Regression Estimates

Figure 8 shows regression estimates for the three end-members over the last 23 Ma. The width of each 95% confidence bands suggests that we can consider these composite records in two parts. Before $\sim$12 Ma, all three composite records are effectively identical with the same pattern occurring in each ocean. After $\sim$12 Ma, the three composite records diverge by up to about 1.5‰.

In general terms, our results confirm well-known behaviour. Circumpolar Deep Water (CPDW) represents a mixture of NADW and recirculated deep water from the Indian and Pacific Oceans. Consequently, CPDW $\delta^{13}$C values lie between those of NADW (characterized by high $\delta^{13}$C and low nutrients) and Indo-Pacific Deep Water (low $\delta^{13}$C and high nutrients). Without any NADW influence, the $\delta^{13}$C of CPDW should decrease to Indo-Pacific values, regardless of how the oceanic inventory of $^{12}$C or $^{13}$C might have changed [*Charles and Fairbanks*, 1992]. Thus the observation that Atlantic, Southern and Pacific Ocean $\delta^{13}$C end-member records coincide prior to $\sim$ 12 Ma suggests that significant NCW production began at about 12 Ma. Detailed age calibration and error analysis strengthens earlier suggestions based on carbon isotopes that NCW production was weak during middle Miocene times (16–11.6 Ma) but became more important after about 12 Ma [*Woodruff and Savin*, 1989, 1991; *Wright et al.*, 1992; *Wright and Miller*, 1993]. The magnitude of a $\delta^{13}$C gradient, or the lack of any such gradient, may also be due to lower whole ocean nutrients [e.g. *Delaney and Boyle*, 1987] and may be the cause

of the similarities between the North Atlantic, Southern and Pacific Ocean composite records during early and middle Miocene times.

Changes in the global carbon reservoir are thought to cause long-period variations in $\delta^{13}$C [*Miller and Fairbanks*, 1985; *Vincent and Berger*, 1985; *Shackleton*, 1987]. These reservoir-related $\delta^{13}$C variations are most noticeable in the period 23–12 Ma. For example, the Monterey Excursion between ∼17.5 Ma and 13.5 Ma is a well-known feature of Miocene benthic $\delta^{13}$C records which is thought to be caused by a period of increased organic carbon burial [*Vincent and Berger*, 1985]. $\delta^{13}$C also decreases between ∼22 and 20 Ma, which may correlate with shallowing of the CCD identified by *van Andel* [1975] and *van Andel et al.* [1975]. *Lyle* [2003] attributes the shallowing of the CCD to warming and expansion of shallow seas due to a 50 m sea-level rise that led to increased sequestration of $CaCO_3$.

There are also short (1–2 Ma) intervals at 19 and 17 Ma when one oceanic mass significantly diverges from another. These anomalous intervals typically involve large negative excursions of Pacific benthic $\delta^{13}$C, suggesting that there was intermittent production of a deep-water source, possibly located in the Antarctic or North Atlantic Oceans, depending on the direction of the $\delta^{13}$C gradient. North Atlantic type surface water that sinks to form deep water is enriched in $^{13}$C, but as deep waters move away from their source region they gradually accumulate organic carbon rich in $^{12}$C from shallow waters. Thus its $\delta^{13}$C signature is gradually reduced as it travels from its source (i.e. water-mass ageing).

From 12–0 Ma, rapid divergence of the end-member curves may mark the beginning of more sustained large volume production of NCW. The North Atlantic end-member oscillates around a constant value from this time onwards, reflecting continuous sinking of water depleted in $^{12}$C by surface productivity. The Pacific Ocean end-member has the lowest values of $\delta^{13}$C during this period. The Southern Ocean end-member fluctuates between North Atlantic and Pacific Ocean values. For the purposes of this paper, we use $\delta^{13}$C as a water-mass tracer and assume that changes in Southern Ocean $\delta^{13}$C are caused by variations in the strength of NCW export from the Norwegian Sea. These variations

can only give an indication of the relative flux of NCW in the Southern Ocean and should not be regarded as a measure of absolute export fluxes.

### 4.1. Estimation of Northern Component Water 0–23 Ma

Following *Wright and Miller* [1996], we wish to use these records to estimate the variation in NCW overflow over the last 23 Ma. According to *Oppo and Fairbanks* [1987], the percentage of NCW present in the Southern Ocean is given by Equation (1). This mixing equation is undoubtedly a simplistic way of representing the relationship between these three water masses, but it can be regarded as a useful starting point. It can only be applied when $\delta^{13}\mathrm{C}_{SO} \geq \delta^{13}\mathrm{C}_{PO}$ and $\delta^{13}\mathrm{C}_{NA} > \delta^{13}\mathrm{C}_{PO}$. Thus before 12 Ma, when all three confidence bands overlap, we cannot calculate %NCW [*contra Wright and Miller*, 1996].

Between 12 and 0 Ma, %NCW can be calculated ($\widehat{NCW}$) and an estimate of its variance is given by

$$\hat{V}^{\widehat{NCW}} = \frac{A}{(\delta^{13}\mathrm{C}_{NA} - \delta^{13}\mathrm{C}_{PO})^2} + \frac{B}{(\delta^{13}\mathrm{C}_{NA} - \delta^{13}\mathrm{C}_{PO})^4} - \frac{2C}{(\delta^{13}\mathrm{C}_{NA} - \delta^{13}\mathrm{C}_{PO})^3} \qquad (3)$$

where $A = \hat{V}^{SO} + \hat{V}^{PO}$, $B = (\delta^{13}\mathrm{C}_{SO} - \delta^{13}\mathrm{C}_{PO})^2(\hat{V}^{NA} + \hat{V}^{PO})$ and $C = (\delta^{13}\mathrm{C}_{SO} - \delta^{13}\mathrm{C}_{PO})\hat{V}^{PO}$ (see *Serfling* [1980] for further details). Here, $\hat{V}^{SO}, \hat{V}^{PO}$ and $\hat{V}^{NA}$ are the estimated variances of $\delta^{13}\mathrm{C}_{SO}$, $\delta^{13}\mathrm{C}_{PO}$ and $\delta^{13}\mathrm{C}_{\mathrm{NA}}$, respectively.

%NCW is shown in Figures 9a and 10. We must emphasize that %NCW is unlikely to decrease to zero at any time during the last 12 Ma and so the percentage range is best thought of as indicating 'weaker' and 'stronger' NCW overflow. When %NCW is close to zero, it may partly indicate movement of the mixing zone northwards or shoaling of the mixing zone such that Southern Ocean sites no longer sit within this zone. During the last 12 Ma, the most striking feature of calculated %NCW is the rapid increase at 6 Ma and decrease at 2 Ma. Other short period variations also appear to be well-resolved.

### 4.2. Evolutive Spectral Analysis

The composite records span a large interval and we expect that amplitudes of different frequency responses to insolation will vary with time. These records have been carefully constructed and are of high sample resolution so it is useful to study changes in power spectra of different orbital periodicities contained within the data. An evolutive spectral analysis technique is used to display temporal changes in the power of different orbital periodicities. To apply this technique, results from the local linear kernel regression are exploited because bandwidths were chosen to reflect sample resolution, enabling short-period cyclicities, where present, to be retained. In some age intervals, there is limited spectral information for orbital frequencies of interest. Evolutive spectra are generated using the Thomson multi-taper method with a time-bandwidth product of 4 and eigenspectra of 6 [*Torrence and Compo*, 1998]. Nonparametric regression estimates were analysed with a sliding window length of 1500 ka and a step size of 125 ka. The shorter %NCW record was analysed with a window length of 625 ka and a step size of 62.5 ka.

Individual records show that, where there is significant data resolution, nonparametric analysis of composite records retains the orbital cyclicities expected from benthic stable isotope records. We have also examined the spectral content of the 0–7 Ma %NCW estimate since there are spectral peaks in the benthic $\delta^{13}$C data whence it is calculated (Figure 10). The presence of obliquity is notable between 3 and 1.6 Ma, although it is present quite consistently across the entire 0–7 Ma interval (Figure 11). This strong obliquity signal suggests that %NCW is sensitive to obliquity forcing. Such a response may be characteristic of either the way carbon cycles respond to insolation forcing in the oceans during Late Neogene times, or a determinant of NCW formation in the Northern Seas. It is interesting to note that the obliquity component of the North Atlantic endmember during this interval decays from a peak around 6.5 Ma and is weak by 5 Ma. In contrast, the Pacific Ocean benthic $\delta^{13}$C record only contains a large obliquity component from ∼3.5 Ma. *Haug et al.* [2005] suggest that changes in the subarctic Pacific halocline, triggered by an obliquity minimum at ∼2.7 Ma, resulted in moisture release and

in the Northern Hemisphere Glaciation (NHG). The %NCW record may be responding to obliquity forcing in the Pacific Ocean beginning around 3 Ma. The timing of changes in obliquity amplitude in the Pacific benthic $\delta^{13}$C record occur before the changes in the surface subarctic Pacific Ocean. The increase in obliquity component in %NCW ∼3 Ma, however, does coincide with Northern Hemisphere Glaciation. The Plio-Pleistocene benthic $\delta^{18}$O stack of *Lisiecki and Raymo* [2005] also shows changes in orbital forcing response, which occurred in conjunction with the climate transition ∼3 Ma. Their data indicate a change in the phase (or lag) of the precession and obliquity components of benthic $\delta^{18}$O with respect to an orbitally forced ice-volume model at this time. *Haug and Tiedemann* [1998] suggest that NHG was caused by a combination of the late Cenozoic cooling trend, Panama Isthmus closure affecting deep-water circulation in the North Atlantic, and finally triggered by favourable obliquity forcing. Recent modelling to test this hypothesis has failed to find support that the delivery of moisture (through closure of the Panama Isthmus) was a precondition for the obliquity trigger [*Klocker et al.*, 2005]. The timing of the impact of closure of the Central American Seaway on deep-water circulation ∼4.6 Ma [*Ravelo et al.*, 2004] also casts doubt on the closure of the Panama Isthmus as the final precondition for obliquity-triggered NHG [*Haug et al.*, 2005]. *Klocker et al.* [2005] suggest that whilst obliquity modulation may be the trigger, the climate system needed different preconditions to allow the long-term build-up of ice in the Northern Hemisphere.

## 5. Iceland Plume Variation?

*Wright and Miller* [1996] suggested that the variation of NCW flux was controlled by vertical motions of the GSR which were in turn controlled by temperature fluctuations within the Iceland Plume. Here we wish to test this hypothesis in the light of our newly calculated %NCW and our study of the associated errors (Figures 9a and 10).

### 5.1. Gateway Closure

Given considerable uncertainties in paleogeographical reconstructions, we are conscious that %NCW variation can be interpreted in various ways. We are also conscious of recent suggestions that orbital forcing may combine with gradual changes in atmospheric and circulation boundary conditions to produce large, long-term changes in parameters such as benthic $\delta^{18}$O and %NCW [e.g. *Haug and Tiedemann*, 1998; *Haug et al.*, 2005]. Here, we restrict ourselves to tectonic explanations, although we acknowledge that there may be other (contributory) causes of %NCW variations.

Two crucial issues affecting NCW production are convective overturning within the Labrador Sea and changes in inter-oceanic communication. The Labrador Sea is evidently an important source of deep water whose temporal evolution is poorly understood. For now, we must assume that its contribution does not vary significantly over the interval of interest. On the other hand, opening and closing of gateways could profoundly influence thermohaline circulation (including Labrador Sea convective overturn) and we must address the gateway issue in more detail.

Two significant gateway closures occur during the interval of interest: progressive closure of the Panama Gateway and final closure of the Tethyan Ocean. In both cases, deep-water circulation patterns and $\delta^{13}$C gradients between the major oceanic basins were undoubtedly affected. Tethyan ocean closure is imprecisely dated but it probably influenced Atlantic deep waters until ∼13 Ma [*Ramsay et al.*, 1998].

Onset of significant NCW production may have been influenced by closure of the Panama Gateway, which gradually separated Atlantic and Pacific oceanic circulation through Miocene-Pliocene times. Global circulation models have been used to suggest that the present-day configuration of global thermohaline circulation is not possible with an open Panama gateway [*Maier-Reimer et al.*, 1990]. If the pathway of warm, salty water associated with the Gulf Stream is forced to the north, it is possible that the Labrador Sea becomes the site of important deep-water production. It is also likely that, whilst deep-

water production was possible in the Norwegian–Greenland Seas prior to the formation of the Panama Isthmus, the flux was significantly increased by the Gulf Stream bringing warm salty surface waters to high latitudes. Both changes could significantly influence the quantity of NCW exported into the Southern Ocean. Our principal consideration here is timing of gateway closure. Foraminiferal stratigraphy of Central America suggests that initial uplift of the Panama Sill occurred at 15–15.9 Ma, although the deep-water connection was probably not severed at this time [*Duque-Caro*, 1990]. Separation of Pacific and Caribbean benthic faunas, following a hiatus at 12.2–13.1 Ma, represents the first evidence for development of a sill which was shallow enough to restrict Atlantic-Pacific deep water-mass exchange [*Duque-Caro*, 1990]. *Nesbitt and Young* [1997] also argue that closure began at about 12 Ma. Some deep water-mass exchange may have continued until 6.7 Ma [*McDougall*, 1996]. Studies of planktonic faunas indicate gradual separation of surface-water flow after this time, suggesting complete divergence of surface-dwelling faunas by 1.8 Ma [*Keller et al.*, 1989]. Others have argued that water depths of less than 100 m were reached by 4.6 Ma based upon surface salinity increases recorded by planktonic foraminfera [*Keigwin*, 1982; *Haug and Tiedemann*, 1998].

In summary, gradual restriction of deep-water flow relatively early in the history of closure of the Panama gateway could have played a role in affecting major NCW production during mid-late Miocene times. Although there is some disagreement about the exact timings of shallowing and closure, the consensus in the literature suggests that shoaling to  100 m occurred at about 4.6 Ma [*Haug and Tiedemann*, 1998] and that complete closure occurred at about 3.5 Ma [*Duque-Caro*, 1990; *Haug and Tiedemann*, 1998; *Frank et al.*, 1999, Figure 10]. Neither event appears to correspond with major changes in the $\delta^{13}$C composite records or %NCW.

### 5.2. Long-Term Subsidence of Greenland-Scotland Ridge

Long-term subsidence of the GSR in response to plate cooling could have exerted a primary control on onset of NCW production [*Vogt*, 1972]. Subsidence histories of the three present-day GSR gateways are considered separately since they have different tectonic histories (Figure 1). The Faroe-Shetland Channel is floored by a continental extensional sedimentary basin. Drilling and seismic imaging by the hydrocarbon industry show that this region subsided rapidly as a result of Early-Middle Cretaceous rifting. It probably remained at, or deeper than, its present depth of $> 1$ km throughout the Cenozoic era, becoming a conduit for deep water by the early Oligocene [*Davies et al.*, 2001]. It is therefore unlikely that subsidence of this gateway has significantly moderated production of NCW during the Neogene period. The Iceland-Faroe Ridge (IFR) is built from overthickened oceanic crust overlain by a thin veneer of sediment 0–400 m thick [*Smallwood et al.*, 1999]. Its elevation at time $t_r$ before present, $e$, can be reconstructed by accounting for plate cooling using

$$e = h_0 + 380(\sqrt{t_a} - \sqrt{t_a - t_r}) \tag{4}$$

where $t_a$ is plate age in Ma, $h_0$ is present elevation in meters, and constant $380\,\mathrm{m\,Ma^{-1/2}}$ is from the oceanic age-depth model [*Stein and Stein*, 1992]. Using a maximum present-day water depth of 500 m and a basement age range of 38–55 Ma [*Smallwood and White*, 2002], the IFR would have been elevated above sea level before 18–15 Ma, in agreement with *Thiede and Eldholm* [1983]. The subsidence history determined from DSDP hole 336 on the northern flank of the ridge is compatible with this interpretation [*Detrick et al.*, 1977]. By 12 Ma, the IFR crest should have been 100–200 m below sea-level. The Denmark Straits are underlain by oceanic crust in the east and by the Greenland passive continental margin further west. Despite its complex basement architecture, subsidence of Denmark Straits basement was probably similar to that of the IFR, since subsidence of 55 Ma oceanic crust approximates post-break-up subsidence of the passive margin and oceanic

crust beneath the eastern part of the straits is about 38 Ma old [*Smallwood and White*, 2002]. A larger source of uncertainty in sea-bed subsidence arises from uncertainty in accumulation history of the 1 km thick sedimentary layer which mantles Denmark Straits basement [*Wright and Miller*, 1996]. Backstripping this sediment layer shows that the seabed may have been a maximum of 500 m deeper than the depth predicted by the simple plate cooling model above, if the entire sediment layer accumulated since the beginning of the Miocene period [Figure 1c of *Jones and Maclennan*, 2005]. It is more likely that this sediment layer accumulated gradually so that the seabed was never much more than 100 m deeper than predicted by Equation (4).

We suggest that subsidence of the Greenland-Scotland Ridge on either side of Iceland exerted a direct control on NCW formation that was as least as significant as closure of the Panama Gateway. At present, more than half of the northward flow of saline surface water travels across the Iceland-Faroe Ridge and more than half of the southward return flow of NADW uses the Denmark Straits [*Hansen et al.*, 2003]. The Iceland-Faroe Ridge, and possibly also the Denmark Straits, probably lay above sea-level prior to middle Miocene times. Limited connection between the Atlantic Ocean and the Greenland-Iceland-Norway Sea served to inhibit formation of NCW north of Iceland. By about 12 Ma, it is likely that water depths in excess of 100 m had been established above the GSR immediately either side of Iceland, which would have allowed saline Atlantic surface water to flow northward, cool, and then sink to form NCW. Initially, return flow of NCW probably occurred through the Faroe-Shetland Channel, which has probably been open and relatively deep since Early Oligocene times [*Davies et al.*, 2001]. Ongoing subsidence of oceanic crust around Iceland through late Miocene time allowed an increasing rate of NCW export through the Denmark Straits, which may account for coeval divergence of the Atlantic and Pacific $\delta^{13}$C records.

### 5.3. Short-Term Uplift/Subsidence of Greenland-Scotland Ridge

Short-lived cycles of uplift and subsidence are superimposed upon the long-term subsidence of the GSR. *Wright and Miller* [1996] used a set of seismic reflection profiles that traverse the Reykjanes Ridge spreading axis to constrain the timing and amplitude of these cycles (Figures 1–3). Variations in depth to oceanic basement define a set of V-shaped ridges that are symmetric about the spreading axis and converge to the south [*Vogt*, 1971]. A coeval set of V-shaped ridges that converge to the north occur along the Kolbeinsey Ridge, north of Iceland (Figure 1), [*Jones et al.*, 2002a]. These V-shaped bathymetric ridges reflect crustal thickness variations that are generated by thermal (and possibly compositional) anomalies within the head of the Iceland Plume that spread outward from Iceland. Fronts of relatively high temperature, propagating outward from Iceland, are associated with dynamic uplift of the overlying plate, since hotter regions are more buoyant. The geometry of the V-shaped ridges alone cannot be used to determine whether outward asthenosphere flow was radial or channelled beneath the spreading axis [*White and Lovell*, 1997; *Jones et al.*, 2002a]. It is more likely that fronts of high temperature propagated radially beneath a horizontal boundary at a depth of about 100 km where a large viscosity increase arises from dewatering of the mantle in the earliest stages of melting [*Ito et al.*, 1999; *Ito*, 2001; *Jones et al.*, 2002a]. Hence, V-shaped ridges formed at the Reykjanes Ridge south of Iceland can be correlated with uplift of the GSR to the west and east of Iceland.

V-shaped ridge bathymetry can be converted into residual depth, which is the difference between the observed depth to oceanic basement and the depth predicted by a half-space cooling model. Depths to oceanic basement are derived from *Talwani et al.* [1971], reported in *Wright and Miller* [1996]. Residual depth directly reflects dynamic support, although features less than about 0.1 Ma in duration may have been modified by faulting and can be regarded as noise. *Wright and Miller* [1996] also presented estimates of accumulation rate of major North Atlantic sediment drifts and estimates of lava extrusion

rates at Iceland as supporting evidence that vertical motion of the GSR affected the flow of NCW. *Jones et al.* [2002a] produced a V-shaped ridge record based on gravity anomalies. The gravity record resembles a smoother version of the residual depth record.

The V-shaped records from residual depth and gravity were originally plotted as functions of time using magnetic anomalies correlated to the timescales of *Berggren et al.* [1985] and *Cande and Kent* [1995], respectively [*Wright and Miller*, 1996; *Jones et al.*, 2002a]. We have placed these records on the astronomical time scale of [*Lourens et al.*, 2004], since we wish to compare them with our %NCW record.

### 5.4. Timing of Uplift at the Major Spill-Points

It is necessary to adjust the V-shaped ridge records to reflect the timing of uplift/subsidence events at locations of deep-water flow over the GSR in order to make a comparison with %NCW. Temperature anomalies that generate the V-shaped ridges propagate radially outward from Iceland, so the timing of associated uplift depends on the propagation speed and radial distance from the plume centre. The propagation speed is determined from the angles between V-shaped ridges and the spreading axis. *Wright and Miller* [1996] measured propagation speeds between 1140 km/Ma for the youngest ridge and 163 km/Ma for their oldest ridge.

The residual depth record was formed at 515 km from the plume center. *Wright and Miller* [1996] adjusted the original record to reflect uplift/subsidence at Iceland itself using a different propagation speed for each ridge. We removed these adjustments to recreate the original record. We then sought a uniform time shift that resulted in a good negative correlation between rapid changes in the slope of residual depth and %NCW. A uniform time shift of +0.11 Ma results in a reasonable negative correlation. Denmark Straits and the Faroe Shetland Channel currently lie 480 km and 760 km from the plume centre, respectively. Using the range of propagation speeds determined by *Wright and Miller* [1996], a time shift of between +0.03 and +0.21 Ma applied to the residual depth

record should predict uplift/subsidence of the Denmark Straits, and a shift of between −0.22 and −1.52 Ma should predict uplift/subsidence of the Faroe Shetland Channel. The velocities found by *Wright and Miller* [1996] progressively increase for each ridge and so the time shift required for the plume anomaly to reach Denmark Straits should be closer to +0.03 Ma for the younger ridges (Ridge 1) and closer to 0.21 Ma for the older ridges (Ridges 3 and 4). The residual depth record has been shifted by +0.11 Ma (Figure 9a) and by +0.21 Ma (Figure 9b) to reflect vertical motions of the Denmark Straits. We have also tried timeshifts which vary with age, as well as automated correlation. In our view, the use of an elastic correction is not yet justified.

Since a reasonable correlation between residual depth and %NCW requires a uniform timeshift of +0.11, we suggest that vertical motions of the Denmark Straits have exerted the most important control on flow of deep water between the Norwegian-Greenland Sea and the Atlantic Ocean during the Neogene period. Comparing the V-shaped ridge gravity record with %NCW supports this conclusion, although the negative correlation is not so striking because the gravity record is smoother than the residual depth record. Note that *Wright and Miller* [1996] and *Jones et al.* [2002a] found that %NCW was sensitive to uplift at Iceland itself. The improved quality of our %NCW record suggests instead that NCW flow is more sensitive to uplift at the Denmark Straits.

## 6. Discussion

Having made appropriate adjustments for the time taken for a hot pulse to reach a distall spill point on the GSR (i.e. the Denmark Straits), we can now compare our revised %NCW record with uplift/subsidence records of Iceland Plume. Plume-related uplift and plate cooling correlate with important changes in %NCW although we acknowledge that other events probably impact %NCW production and export during the Neogene period.

### 6.1. %NCW between 23 and 12 Ma

Fluctuations in %NCW over the interval 23–12 Ma are inconclusive because the three composite $\delta^{13}$C records overlap within error. There is evidence for small inter-oceanic $\delta^{13}$C gradients but carbon isotopes do not necessarily reveal the presence of large-scale meridional circulation. Higher resolution data may help to reduce the width of confidence bands and to increase the precision of correlation between end-members, but it is unlikely that large $\delta^{13}$C gradients will be uncovered. The divergence of North Atlantic and Pacific Ocean $\delta^{13}$C records at 12 Ma is attributed to the production of large volumes of NCW in the North Atlantic/Norwegian Greenland Sea. Deep-water formation patterns are more easily understood by examining statistically significant %NCW variations.

### 6.2. Late Miocene to Present %NCW Variations: One Simple Cause?

Since ∼12 Ma, large amounts of deep water have formed episodically in the North Atlantic Ocean, causing $\delta^{13}$C records for the North Atlantic and Pacific Oceans to diverge (Figure 8). Southern Ocean data fluctuate between these two end-members. Between 11 and 6 Ma, estimates of %NCW are reliable and negatively correlate with vertical motions of the GSR (Figure 9). This correlation is particularly striking when the residual depth record is shifted to reflect uplift and subsidence of the Denmark Straits. Thus plume-related uplift of Iceland appears to significantly restrict the amount of deep water which spills over the GSR at the Denmark Straits. Its impact would be greater than simply reducing the 5.6 Sv of water which currently overflow the ridge, since overflowed water entrains intermediate waters which help to increase the flux of present-day Lower North Atlantic Deep Water [*Dickson and Brown*, 1994]. A weaker correlation between this %NCW record and subsidence of the Faroe Shetland Channel suggests that the Denmark Straits controlled large-volume NCW production.

Figure 10 shows %NCW for the last 8 Ma when the highest resolution records exist for each of the three end-members. Several broad-scale features are of interest. At 6

Ma, there was a rapid increase in %NCW, which we interpret as an increase in NCW production rather than a proportional increase in Southern Component Water. Another rapid increase occurred at 5.2 Ma. These changes precede a sustained interval of NCW production which continues until 2.7 Ma. We attribute the increase in %NCW at 6 Ma to reduced dynamic support at the Denmark Straits. This reduction is inferred from the trough between Ridges 1 and 2. *Wold* [1994] has highlighted a dramatic increase in sedimentary flux across the GSR at ∼6 Ma, and a slight decrease at ∼2 Ma, both of which correlate very well with an increase and decrease in %NCW, respectively.

From 2.7 Ma onwards, the proportion of NCW in the Southern Ocean diminishes steadily until ∼1.9 Ma. Intensification of the Northern Hemisphere Glaciation and stagnation of waters in the northern seas also occurred at this time [*Maslin et al.*, 1998]. This time interval coincides with the formation of V-shaped Ridge 1 in response to an increase in temperature within the Iceland Plume head. We suggest that the associated dynamic uplift of the GSR decreased southward overflow of deep water from the NGS, and reduced strength of thermohaline circulation. Stagnation of bottom waters and poor carbonate preservation reported by *Henrich et al.* [2002] ensued. Reduction in NCW also reduced latitudinal heat transport, thereby rapidly increasing the areal extent of Northern Hemisphere Glaciation.

The composite benthic $\delta^{18}$O record suggests that, despite large fluctuations in the proportion of NCW in the Southern Ocean, periods of sudden increase or decrease in %NCW are not generally associated with significant changes in deep-water $\delta^{18}$O composition. Thus long-term changes in the strength of NCW do not obviously correlate with major changes in the Earth's glaciation history. However, two of the major decreases in benthic $\delta^{18}$O, at ∼15 and ∼3.6 Ma, do match the rapid growth of the two biggest V-shaped ridges formed during the Neogene period (Ridges 1 and 3). Our records suggest that changes in %NCW, caused by the formation of Ridge 1, are associated with an increase in Northern Hemisphere Glaciation at ∼3.6 Ma [*Wright and Miller*, 1996]. The possibility remains,

given the uncertainties associated with %NCW prior to ∼12 Ma, that Ridge 3 interrupted NCW production and export from the Norwegian-Greenland Seas, providing moisture for the mid-Miocene growth in the Antarctic ice sheet [*Schnitker*, 1980].

### 6.3. Sensitivity of %NCW to Data Choice

Although %NCW generally correlates well with Iceland Plume activity, there was initially a significant mismatch at 7 Ma (Figure 9). When composite records are scrutinized, it is clear that the 7 Ma peak in %NCW is caused by an increase in the Southern Ocean $\delta^{13}$C composite record that is controlled by a small number of high values (Figure 8). These high values of $\delta^{13}$C come from two sets of analyses carried out on ODP site 704 at 2.5 km depth (Figure 12). These analyses diverge from the trends in ODP site 1088 and DSDP site 360 (at depths of 2 and 3 km, respectively). There is further disagreement between the two Site 704 datasets, *Müller et al.* [1991] and *Wright et al.* [1991], where Müller's data is generally positively offset from the other data. *Billups et al.* [2002] states that there is no obvious environmental cause for the differences between the two Site 704 datasets that sample the late Miocene period. We therefore suggest that data from Site 1088 (and Site 360) better reflect the benthic $\delta^{13}$C composition of the Southern Ocean through this interval. If Site 704 values are removed, causing the record to be based on Site 1088 during the late Miocene, the %NCW peak at 7 Ma is considerably diminished (Figure 9). One cause of the difference in $\delta^{13}$C between Site 704 and Sites 360 and 1088 may be small changes in the geometry of the mixing front between NADW and CDW [*Billups et al.*, 2002]. The differences between Site 704 and Sites 360 and 1088 highlight the importance of choosing appropriate data for each of the benthic $\delta^{13}$C end-members, since %NCW is sensitive to changes in data, especially in the Southern Ocean. Close examination of the records reveals no other region of overlap between datasets with such a large discrepancy.

## 7. Conclusions

In order to test *Wright and Miller* [1996]'s assertion that temporal variations associated with the Iceland Plume controlled overflow of Northern Component Water at the Greenland Iceland Ridge, we have assembled composite $\delta^{13}$C records for the Atlantic, Southern and Pacific Oceans. These composite records were calibrated with the astronomical timescale and fitted with nonparametric functions. We paid particular attention to the construction of confidence bands.

We have then used these three composite records to calculate the percentage overflow of Northern Component Water. There is no evidence for significant NCW overflow before 12 Ma since the three oceanic end-members overlap within error. A marked divergence of the three $\delta^{13}$C records at 12 Ma indicates the onset of significant NCW overflow which may be related to submergence of the Iceland-Faroe Ridge caused by lithospheric plate cooling. This inference could be more rigorously tested by analyzing the detailed subsidence histories of the Greenland-Scotland Ridge, which requires deep drilling on the Iceland-Faroe Ridge and in the Denmark Straits.

Despite the many *caveats* concerning the use of $\delta^{13}$C records to reconstruct overflow of NCW, and despite uncertainties surrounding the importance of Labrador Sea convective overturn and the timing of Panama Gateway closure, there is a remarkably good correlation between %NCW and inferred vertical motions of the Denmark Straits. This correlation suggests that short-term (order 2–3 Ma) fluctuations of %NCW after 12 Ma are controlled by vertical motions of the GSR, which are generated by temperature fluctuations associated with the Iceland Plume, vindicating the Wright and Miller hypothesis. Uplift fluctuations are likely to be several hundred metres but detailed modelling is required to confirm this influence. The match between short-term features of the %NCW record and the V-shaped ridge record strengthens the suggestion that the Greenland-Scotland Ridge also controlled onset of NCW production in the longer term. Nonetheless,

more sustained production of NCW may only occur after closure of the Panama Isthmus in order to supply warm salty surface water to high northern latitudes.

Intensification of Northern Hemisphere Glaciation at 2.7 Ma may be related to the restriction in %NCW in response to dynamic uplift associated with the youngest V-shaped ridge. A reduction in %NCW at 2.7 Ma may coincide with an increase in obliquity forcing at 2.8 Ma. This reduction may indicate increased dominance of NCW, which has a strong obliquity component, in controlling circulation and glaciation. These hypotheses could, in part, be tested by detailed examination of North Atlantic ODP sites. Finally, the statistical techniques used to generate confidence bands for non-uniformly sampled isotopic data may be of more general application in paleoceanography.

**Acknowledgments.** We warmly acknowledge the help of N. Shackleton, K. Billups and H. Pfuhl who very generously provided access to unpublished data. L. Lourens, J. Ogg, H. Luterbacher and N. Shackleton gave us astronomical time scales and H. Pälike helped construct evolutive spectral analyses. We also thank S. Crowhurst, G. Edwards, C. Lear, D. Lyness, D. M$^c$Kenzie and R. Rickaby for their considerable help and interest. The thoughtful comments of two anonymous reviewers and the editor, Laurent Labeyrie, greatly improved the manuscript. Figures were produced using the GMT software package. Department of Earth Sciences Contribution Number 8273.

## References

Berggren, W. (1992), Neogene planktonic foraminifer magnetostratigraphy of the southern Kerguelen Plateau (Sites 747, 748 and 751), in *Proceedings of the Ocean Drilling Program, Scientific Results*, vol. 120, pp. 631–647.

Berggren, W., D. V. Kent, and J. A. van Couvering (1985), The Neogene: Part 2, Neogene geochronology and chronostratigraphy, in *The Chronology of the Geological record*, edited by N. Snelling, no. 10 in Geological Society Memoir, pp. 211–260, Blackwell

Scientific Publications.

Billups, K. (2002), Late Miocene through early Pliocene deep water circulation and climate change viewed from the sub-Antarctic South Atlantic, *Palaeogeography, Palaeoclimatology, Palaeoecology*, *185*, 287–307.

Billups, K., A. C. Ravelo, and J. C. Zachos (1997), Early Pliocene deep-water circulation: stable isotope evidence for enhanced Northern Component Deep Water, in *Proceedings of the Ocean Drilling Program, Scientific Results*, vol. 154, pp. 319–330.

Billups, K., A. Ravelo, and J. Zachos (1998), Early Pliocene deep water circulation in the western equatorial Atlantic: implications for high-latitude climate change, *Paleoceanography*, *13*(1), 84–95.

Billups, K., J. Channell, and J. Zachos (2002), Late Oligocene to early Miocene geochronology and paleoceanography from the subantarctic South Atlantic, *Paleoceanography*, *17*(1), 4–1–4–11.

Billups, K., H. Pälike, J. Channell, J. Zachos, and N. Shackleton (2004), Astronomic calibration of the late Oligocene through early Miocene geomagnetic polarity time scale, *Earth and Planetary Science Letters*, *224*, 33–44.

Broecker, W., and T. Peng (1982), *Tracers in the Sea*, Lamont-Doherty Geological Observatory, Palisades, NY.

Burton, K., H. Ling, and R. O'Nions (1997), Closure of the Central American Isthmus and its effect on deep-water formation in the North Atlantic, *Nature*, *386*, 382–385.

Cande, S., and D. Kent (1995), Revised calibration of the geomagnetic polarity timescale for the Late Cretaceous and Cenozoic, *Journal of Geophysical Research*, *100*(B4), 6093–6095.

Carroll, R., D. Ruppert, and L. Stefanski (1995), *Measurement Error in non-linear models*, Chapman and Hall, London.

Charles, C. D., and R. G. Fairbanks (1992), Evidence from Southern Ocean sediments for the effect of North Atlantic deep-water flux on climate, *Nature*, *355*, 416–419.

Claeskens, G., and I. van Keilegom (2003), Bootstrap confidence bands for regression curves and their derivatives, *The Annals of Statistics*, *31*(6), 1852–1884.

Clement, B. M., and F. Robinson (1986), The magnetostratigraphy of Leg 94 sediments, in *Initial Reports of the Deep Sea Drilling Project*, vol. 94, Part 2, pp. 635–650.

Cook, J., and L. Stefanski (1994), Simulation-extrapolation estimation in parametric measurement error models, *Journal of the American Statistical Association*, *89*, 1314–1328.

Corfield, R. M., and J. E. Cartlidge (1993), Oxygen and carbon isotope stratigraphy of the middle Miocene, Holes 805B and 806B, in *Proceedings of the Ocean Drilling Program, Scientific Results*, vol. 130, pp. 307–322.

Curry, W., and K. Miller (1989), Oxygen and carbon isotopic variation in Pliocene benthic foraminifers of the equatorial Atlantic, in *Proceedings of the Ocean Drilling Program, Scientific Results*, vol. 108, pp. 157–166.

Davies, R., J. Cartwright, J. Pike, and C. Line (2001), Early Oligocene initiation of North Atlantic Deep Water formation, *Nature*, *410*, 917–920.

Delaney, M., and E. Boyle (1987), Cd/Ca in late Miocene benthic foraminifera and changes in the global organic carbon budget, *Nature*, *330*(6144), 156–159.

Detrick, R., J. Sclater, and J. Thiede (1977), The subsidence of aseismic ridges, *Earth and Planetary Science Letters*, *34*, 185–196.

Dickson, R., and J. Brown (1994), The production of North Atlantic Deep Water: sources, rates and pathways, *Journal of Geophysical Research*, *99*(C6), 12,319–12,341.

Duque-Caro, H. (1990), Neogene stratigraphy, paleoceanography and paleobiogeography in northwest South America and the evolution of the Panama Seaway, *Palaeoceanography, Palaeoclimatology, Palaeoecology*, *77*, 203–234.

Ellis, C. H. (1975), Calcareous nannofossil biostratigraphy - Leg 31, DSDP, in *Intial Reports of the Deep Sea Drilling Project*, vol. 31, pp. 655–676.

Fan, J., and I. Gijbels (1996), *Local Polynomial Modelling and its Applications*, chap. 2, pp. 16–19, Chapman and Hall, London.

Frank, M., B. Reynolds, and R. O'Nions (1999), Nd and Pb isotopes in Atlantic and Pacific water masses before and after closure of the Panama gateway, *Geology*, *27*(12), 1147–1150.

Gartner, S., and J. Chow (1985), Calcareous nannofossil biostratigraphy: Deep Sea Drilling Project Leg 85, eastern equatorial Pacific, in *Initial Reports of the Deep Sea Drilling Project*, vol. 85, pp. 609–619.

Graham, D. W., B. Corliss, M. Bender, and L. Keigwin (1981), Carbon and oxygen isotopic disequilibria of recent deep-sea benthic foraminifera, *Marine Micropaleontology*, *6*, 483–497.

Hailwood, E., and B. Clement (1991), Magnetostratigraphy of Sites 703 and 704, Meteor Rise, southeastern South Atlantic, in *Proceedings of the Ocean Drilling Program Scientific Results*, vol. 114, pp. 367–386.

Hansen, B., S. Østerhus, H. Hátún, R. Kristiansen, and M. Larsen (2003), The Iceland–Faroe inflow of Atlantic water to the Nordic seas, *Progress in Oceanography*, *59*, 443–474.

Haug, G. H., and R. Tiedemann (1998), Effect of the formation of the Isthmus of Panama on Atlantic Ocean thermohaline circulation, *Nature*, *393*, 673–676.

Haug, G. H., et al. (2005), North Pacific seasonality and the glaciation of North Atmerica 2.7 million years ago, *Nature*, *433*, 821–825.

Heider, F., B. Leitner, and H. Inokuchi (1992), High southern latitude magnetostratigraphy and rock magnetic properties of sediments from Sites 747, 749 and 751, in *Proceedings of the ODP, Scientific Results*, vol. 120, pp. 225–245, Ocean Drilling Program.

Henrich, R., K. Baumann, R. Huber, and H. Meggers (2002), Carbonate preservation records of the past 3 Myr in the Norwegian Greenland Sea and the northern North Atlantic: implications for the history of NADW production, *Marine Geology*, *184*, 17–39.

Hodell, D., J. Curtis, F. Sierro, and M. Raymo (2001), Correlation of late Miocene to early Pliocene sequences between the Mediterranean and North Atlantic, *Paleoceanography*, *16*, 155–163.

Hodell, D. A., and P. F. Ciesielski (1991), Stable isotopic and carbonate stratigraphy of the Late Pliocene and Pleistocene of Hole 704A: eastern subantarctic South Atlantic, in *Proceedings of the Ocean Drilling Porgram, Scientific Results*, vol. 114, pp. 409–435.

Imbrie, J., J. Hays, D. Martinson, A. McIntyre, A. Mix, J. Morley, N. Pisias, W. Prell, and N. Shackleton (1984), The orbital theory of Pleistocene climate: support from a revised chronology of the marine $\delta^{18}$o record, *NATO AS Series C, Math Phys. Sci*, *126*, 269–305.

Ito, G. (2001), Reykjanes "V"-shaped ridges originating from a pulsing and dehydrating mantle plume, *Nature*, *411*, 681–684.

Ito, G., Y. Shen, G. Hirth, and C. J. Wolfe (1999), Mantle flow, melting, and dehydration of the Iceland mantle plume, *Earth and Planetary Science Letters*, *165*(1), 81–96.

Jenkins, D. G. (1978), Neogene planktonic foraminiferas from DSDP Leg 40 Sites 360 and 362 in the southeastern Atlantic, in *Initial Reports of the Deep Sea Drilling Project*, vol. 40, pp. 723–740.

Jones, S., and J. Maclennan (2005), Crustal flow beneath Iceland, *Journal of Geophysical Research*, *110*, doi:10.1029/2004JB003592.

Jones, S. M., N. White, and J. Maclennan (2002a), V-shaped ridges around Iceland: Implications for spatial and temporal patterns of mantle convection, *Geochemistry Geophysics Geosystems $G^3$*, *3*(10).

Jones, S. M., et al. (2002b), Present and past influence of the Iceland Plume on sedimentation, in *Exhumation of the North Atlantic Margin: Timing, Mechanisms and Implications for Petroleum Exploration*, edited by A. Doré et al., no. 196 in Special Publications, pp. 13–25, Geological Society of London.

Katz, M. E., D. Katz, J. Wright, K. Miller, D. Pak, N. Shackleton, and E. Thomas (2003), Early Cenozoic benthic foraminiferal isotopes: species reliability and interspecies correction factors, *Paleoceanography*, *18*(2), 1024.

Keigwin, L. (1982), Isotope paleoceanography of the Caribbean and east Pacific: role of Panama uplift in late Neogene time, *Science*, *217*, 350–353.

Keigwin, L., M.-P. Aubry, and D. Kent (1986), North Atlantic late Miocene stable-isotope stratigraphy, biostratigraphy, and magnetostratigraphy, in *Initial Reports of the Deep Sea Drilling Project Leg 94*, vol. 94, pp. 935–963.

Keigwin, L. D. (1984), Stable isotope results on upper Miocene and Lower Pliocene foraminifers from Hole 552A, in *Initial Reports of the Deep Sea Drilling Project*, vol. 81, pp. 595–597.

Keller, G., C. Zenker, and S. Stone (1989), Late Neogene history of the Caribbean gateway, *Journal of South American Earth Science*, *2*, 73–108.

Klocker, A., M. Prange, and M. Schulz (2005), Testing the influence of the Central American Seaway on orbitally forced Northern Hemisphere glaciation, *Geophysical Research Letters*, *32*, doi:10.1029/2004GL021564.

Kroopnick, P. (1985), The distribution of $^{13}$c of $\sigma co_2$ in the world oceans, *Deep-Sea Research Part A*, *32*(1), 57–84.

Kuijpers, A., B. Hansen, V. Huhnerbach, B. Larsen, T. Nielsen, and F. Werner (2002), Norwegian Sea overflow through the Faroe–Shetland gateway as documented by its bedforms, *Marine Geology*, *188*(1–2), 147–164.

Lear, C. H., Y. Rosenthal, and J. Wright (2003), The closing of a seaway: ocean water masses and global climate change, *Earth and Planetary Science Letters*, *210*, 425–436.

Lisiecki, L. E., and M. E. Raymo (2005), A Pliocene-Pleistocene stack of 57 globally distributed benthic $\delta^{18}$o records, *Paleoceanography*, *20*, doi:10.1029/2004PA001071.

Lourens, L., F. J. Hilgen, J. Laskar, N. Shackleton, and D. Wilson (2004), *A Geologic Time Scale 2004*, chap. 21: The Neogene Period, pp. 409–440, Cambridge University

Press, UK.

Lyle, M. (2003), Neogene carbonate burial in the Pacific Ocean, *Paleoceanography*, *18*(3), doi:10.1029/2002PA000777.

Mackensen, A., H. Hubberten, T. Bickert, G. Fischer, and D. Fuetterer (1993), The $\delta^{13}$c in benthic foraminiferal tests of Fontbotia wuellerstorfi (Schwager) relative to the $\delta^{13}$c of dissolved inorganic carbon in Southern Ocean deep water; implications for glacial ocean circulation models, *Paleoceanography*, *8*(5), 587–610.

Maier-Reimer, E., U. Mikolajewicz, and T. Crowley (1990), Ocean general circulation model sensitivity experiment with an open Central American Isthmus, *Paleoceanography*, *5*, 349–366.

Maslin, M., X. Li, M. Loutre, and A. Berger (1998), The contribution of orbital forcing to the progressive intensification of Northern Hemisphere Glaciation, *Quaternary Science Review*, *17*, 411–426.

McDougall, K. (1996), Benthic foraminiferal response to the emergence of the Isthmus of Panama and coincident paleoceanographic changes, *Marine Micropaleontology*, *28*, 133–169.

Mikolajewicz, U., and T. Crowley (1997), Response of a coupled ocean/energy balance model to restricted flow through the Central American Isthmus, *Paleoceanography*, *12*, 429–441.

Miller, K., and B. Tucholke (1983), Development of Cenozoic abyssal circulation south of the Greenland-Scotland Ridge, in *Structure and development of the Greenland-Scotland Ridge*, edited by M. Bott, S. Saxov, M. Talwani, and J. Thiede, pp. 549–589, Plenum Press, New York.

Miller, K. G., and R. G. Fairbanks (1985), *The carbon cycle and atmospheric $CO_2$: natural variations Archean to Present*, vol. 32, chap. Oligocene to Miocene carbon isotope cycles and abyssal circulation change, pp. 469–486, AGU, Washington, D.C.

Miller, K. G., R. G. Fairbanks, and E. Thomas (1987), Benthic foraminiferal carbon isotopic records and the development of abyssal circulation in the eastern North Atlantic, in *Initial Reports of the Deep Sea Drilling Project*, vol. 94, pp. 981–995.

Miller, K. G., M. D. Feigenson, J. D. Wright, and B. M. Clement (1991), Miocene isotope reference section, Deep Sea Drilling Project Site 608: an evaluation of isotope and biostratigraphic resolution, *Paleoceanography*, *6*(1), 33–52.

Mix, A., and N. Shackleton (1995), Benthic foraminiferal stable isotope stratigraphy of Site 846: 0–1.8 Ma, in *Proceedings of the Ocean Drilling Program, Scientific Results*, vol. 138, pp. 839–854.

Müller, D. W., D. Hodell, and P. Ciesielski (1991), Late Miocene to Earliest Pliocene (9.8-4.5 Ma) paleoceanography of the subantarctic southeast Atlantic: stable isotopic, sedimentologic, and microfossil evidence, in *Proceedings of the Ocean Drilling Program, Scientific Results*, vol. 114, pp. 459–474.

Nesbitt, H. W., and G. M. Young (1997), Sedimentation in the Venezuelan Basin, circulation in the Caribbean Sea, and onset of Northern Hemisphere Glaciation, *Journal of Geology*, *105*(531–544).

Oppo, D., M. Raymo, G. Lohmann, A. Mix, J. Wright, and W. Prell (1995), A $\delta^{13}$C record of Upper North Atlantic Deep Water during the past 2.6 million years, *Paleoceanography*, *11*(3), 373–394.

Oppo, D. W., and R. G. Fairbanks (1987), Variability in the deep and intermediate water circulation of the Atlantic Ocean during the past 25,000 years: northern hemisphere modulation of the Southern Ocean, *Earth and Planetary Science Letters*, *86*, 1–15.

Pfuhl, H., and N. Shackleton (2004), Two proximal, high-resolution records of foraminiferal fragmentation and their implications for changes in dissolution, *Deep-Sea Research I*, *51*(6), 809–832, doi:10.10167j.dsr.2004.02.003.

Pfuhl, H. A., and N. I. McCave (2004), Integrated age models for the early Oligocene-early Miocene, sites 1168 and 1170-1172, in *Proceedings of the Ocean Drilling Program,*

*Scientific Results (CD-ROM)*, vol. 189, Ocean Drilling Program.

Pisias, N., N. J. Shackleton, and M. A. Hall (1985), Stable isotope and calcium carbonate records from hydraulic piston cored Hole 514A: high resolution records from the middle Miocene, in *Initial Reports of the DSDP*, vol. 85, pp. 735–748.

Rahmstorf, S. (2002), Ocean circulation and climate during the past 120,000 years, *Nature*, *419*(6903), 207–214.

Ramsay, A. T., C. W. Smart, and J. C. Zachos (1998), A model of early to middle Miocene deep ocean circulation for the Atlantic and Indian Oceans, in *Geological evolution of ocean basins: results from the Ocean Drilling Program*, edited by A. Cramp, C. MacLeod, S. Lee, and E. Jones, no. 131 in Geological Society of London Special Publications, pp. 55–70, Geological Society, London.

Ravelo, A., D. Andreason, M. Lyle, A. Olivarez Lyle, and M. Wara (2004), Regional climate shifts caused by gradual global cooling in the Pliocene epoch, *Nature*, *429*, 263–267.

Raymo, M., D. Hodell, and E. Jansen (1992), Response of deep ocean circulation to initiation of Northern Hemisphere Glaciation (3-2 Ma), *Paleoceanography*, *7*(5), 645–672.

Ruddiman, W. (2001), *Earth's climate: past and future*, chap. 11, pp. 235–253, W.H. Freeman and Company.

Ruddiman, W., M. E. Raymo, D. Martinson, B. Clement, and J. Backman (1989), Pleistocene evolution: northern hemisphere ice sheets and North Atlantic Ocean, *Paleoceanography*, *4*(4), 353–412.

Samworth, R., and H. R. Poore (2005), Understanding past ocean circulations: a non-parametric regression case study, *Statistical Modelling*, *5*, 289–307.

Savin, S. M., R. Douglas, G. Keller, J. Killingley, L. Shaughnessy, M. Sommer, E. Vincent, and F. Woodruff (1981), Miocene benthic foraminiferal isotope records: a synthesis, *Marine Micropaleontology*, *6*, 423–450.

Schmitz Jr., W. J., and M. S. McCartney (1993), On the North Atlantic circulation, *Reviews of Geophysics*, *31*(1), 29–49.

Schnitker, D. (1980), North Atlantic oceanography as possible cause of Antarctic glaciation and eutrophication, *Nature*, *284*, 615–616.

Serfling, R. (1980), *Approximation theorems of Mathematical Statistics*, chap. 3, p. 122, Wiley, New York.

Shackleton, N. (1987), The carbon isotope record of the Cenozoic: history of organic carbon burial and of oxygen in the ocean and atmosphere, in *Marine Petroleum Source Rocks*, pp. 423–434.

Shackleton, N., and M. Hall (1984), Oxygen and carbon isotope stratigraphy of Deep Sea Drilling Project Hole 552A: Plio-Pleistocene glacial history, in *Initial Reports of the Deep Sea Drilling Project*, vol. 81, pp. 599–610.

Shackleton, N., and N. Pisias (1985), Atmospheric carbon dioxide, orbital forcing, and climate, in *The carbon cycle and atmospheric $CO_2$: natural variations Archean to present*, edited by E. Sundquist and W. Broecker, no. 32 in Geophysical Monograph, pp. 303–317, American Geophysical Union. Washington, DC, United States.

Shackleton, N., A. Berger, and W. Peltier (1990), An alternative astronomical calibration of lower Pleistocene timescale based on ODP Site 677, *Transactions of the Royal Society of Edinburgh: Earth Sciences*, *81*, 251–261.

Shackleton, N., S. Crowhurst, T. Hagelberg, N. Pisias, and D. Schneider (1995a), A new Late Neogene Time Scale: application to Leg 138 Sites, in *Proceedings of the Ocean Drilling Program, Scientific Results*, vol. 138, pp. 73–101.

Shackleton, N., M. Hall, and D. Pate (1995b), Pliocene stable isotope stratigraphy of Site 846, in *Proceedings of the Ocean Drilling Program, Scientific Results*, vol. 138, pp. 337–355.

Shackleton, N. J., and S. Crowhurst (1997), Sediment fluxes based on an orbitally tuned time scale 5 Ma to 14 Ma, Site 926, in *Proceedings of the Ocean Drilling Program,*

*Scientific Results*, pp. 69–82.

Shipboard Scientific Party (1975), Site 289, in *Initial Reports of the Deep Sea Drilling Project*, vol. 30, pp. 231–398.

Shipboard Scientific Party (1999), Site 1088, in *Proceedings of the Ocean Drilling Program, Initial Reports*, vol. 177, pp. 1–36 [CD–ROM].

Smallwood, J., and R. White (2002), Ridge-plume interaction in the North Atlantic and its influence on continental breakup and seafloor spreading, in *The North Atlantic Igneous Province: stratigraphy, tectonic, volcanic and magmatic processes*, *Geological Society Special Publications*, vol. 197, edited by D. Jolley and B. Bell, pp. 15–37, Geological Society, London.

Smallwood, J. R., R. K. Staples, K. Richardson, and R. White (1999), Crust generated above the Iceland mantle plume: From continental rift to oceanic spreading center, *Journal of Geophysical Researches*, *104* (B10), 22,885–22,902.

Srinivasan, M., and J. Kennett (1981), Neogene planktonic foramaniferal biostratigraphy and evolution: equatorial to subantarctic South Pacific, *Marine Micropaleontology*, *6*, 499–533.

Stein, C., and S. Stein (1992), Implications for ridges and transforms of a hotter, thinner lithosphere, *EOS, Transactions*, *73*, 550.

Takayama, T. (1993), Notes on Neogene calcareous nannofossil biostratigraphy of the Ontong Java Plateau and size variations of Reticulofenestra coccoliths, in *Proceedings of the Ocean Drilling Program, Scientific Results*, vol. 130, pp. 179–229.

Talwani, M., C. Windisch, and M. Langseth (1971), Reykjanes Ridge crest: a detailed geophysical study, *Journal of Geophysical Research*, *76*, 473–517.

Thiede, J., and O. Eldholm (1983), Speculation about the paleodepth of the Greenland-Scotland Ridge during Late Mesozoic and Cenozoic times, in *Structure and development of the Greenland-Scotland Ridge*, edited by M. Bott, S. Saxov, M. Talwani, and J. Thiede, pp. 445–456, Plenum Press, New York.

Tiedemann, R., and S. Franz (1997), Deep water circulation, chemistry and terrigenous sediment supply in the equatorial Atlantic during the Pliocene, 3.3-2.6 ma and 5.4-5 ma, in *Proceedings of the Ocean Drilling Program*, vol. 154, pp. 299–318.

Torrence, C., and G. P. Compo (1998), A practical guide to wavelet analaysis, *Bulletin of the American Meteorological Society*, *79*(1), 61–78.

van Andel, T. (1975), Mesozoic/Cenozoic calcite compensation depth and the global distribution of calcareous sediments, *Earth and Planetary Science Letters*, *26*, 187–194.

van Andel, T., et al. (1975), Cenozoic history and paleoceanography of the central equatorial Pacific Ocean, in *Memoirs of the Geological Society of America*, vol. 143, pp. 89–102, Geological Society of America, Boulder, Colorado.

Vincent, E., and W. Berger (1985), Carbon dioxide and polar cooling in the Miocene: the Monterey Hypothesis, in *The carbon cycle and atmospheric $CO_2$: natural variations Archean to Present*, *Geophysical Monograph Series*, vol. 32, edited by E. Sunquist and W. Broecker, pp. 455–468, AGU, Washington, D.C.

Vogt, P. (1971), Asthenosphere motion recorded by the ocean floor south of Iceland, *Earth Planetary Science Letters*, *13*, 153–160.

Vogt, P. (1972), The Faeroe–Iceland–Greenland aseismic ridge and the western boundary undercurrent, *Nature*, *239*, 79–81.

White, N., and B. Lovell (1997), Measuring the pulse of a plume with the sedimentary record, *Nature*, *387*, 888–891.

Whitman, J. M., and W. H. Berger (1993), Pliocene-Pleistocene carbon isotope record, Site 586, Ontong Java Plateau, in *Proceedings of the Ocean Drilling Program, Scientific Results*, vol. 130, pp. 333–348.

Wold, C. (1994), Cenozoic sediment accumulation on drifts in the northern North Atlantic, *Paleoceanography*, *9*, 917–941.

Woodruff, F., and S. M. Savin (1989), Miocene deepwater oceanography, *Paleoceanography*, *4*(10), 87–140.

Woodruff, F., and S. M. Savin (1991), Mid-Miocene isotope stratigraphy in the deep sea: high-resolution correlations, paleoclimatic cycles, and sediment preservation, *Paleoceanography*, *6*(6), 755–806.

Wright, J. D., and K. G. Miller (1992), Miocene stable isotope stratigraphy, Site 747, Kerguelen Plateau, in *Proceedings of the Ocean Drilling Program, Scientific Results*, vol. 120, pp. 855–864.

Wright, J. D., and K. G. Miller (1993), *The Antarctic paleoenvironment; a perspective on global change; Part two*, chap. Southern Ocean influences on late Eocene to Miocene deepwater circulation, pp. 1–25, American Geophysical Union. Washington, DC, United States.

Wright, J. D., and K. G. Miller (1996), Control of North Atlantic Deep Water circulation by the Greenland-Scotland Ridge, *Paleoceanography*, *11*(2), 157–170.

Wright, J. D., K. G. Miller, and R. G. Fairbanks (1991), Evolution of modern deepwater circulation: evidence from the late Miocene Southern Ocean, *Paleoceanography*, *6*(2), 275–290.

Wright, J. D., et al. (1992), Early and middle Miocene stable isotopes: implications for deepwater circulation and climate, *Paleoceanography*, *7*(3), 357–389.

Xia, Y. (1998), Bias-corrected confidence bands in nonparametric regression, *Journal of the Royal Statistical Society, Series B*, *60*, 797–811.

Zachos, J. C., N. Shackleton, J. Revenaugh, H. Pälike, and B. Flower (2001), Climate response to orbital forcing across the Oligocene-Miocene boundary, *Science*, *292*, 274–278.

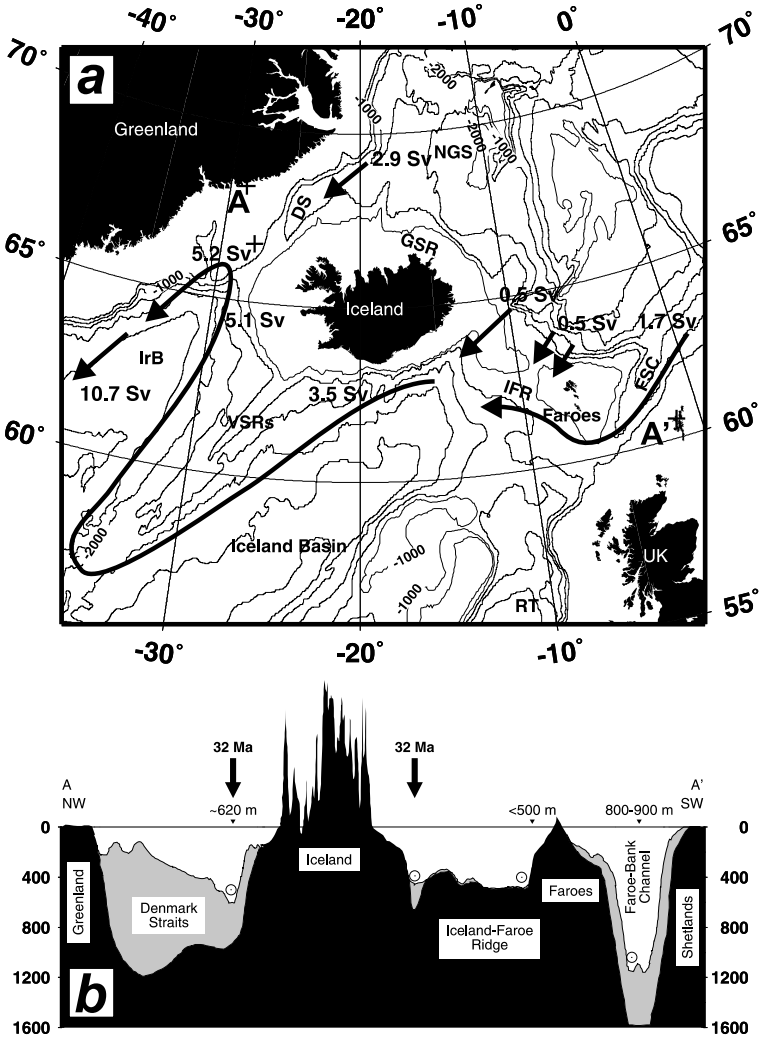


**Figure 1.** (a) Bathymetric map of North Atlantic Ocean. Principal features include Greenland-Scotland Ridge (GSR), Iceland-Faroe Ridge (IFR), Faroe-Shetland Channel (FSC), Rockall Trough (RT), Denmark Straits (DS), Norwegian-Greenland Sea (NGS) and Irminger Basin (IrB). V-shaped ridges (VSRs) are prominent to southwest of Iceland (see Figure 2). Arrows = deep-water currents which overflow GSR. Fluxes are in Sverdrups (1 Sv = $1 \times 10^6 m^3$) beside respective arrow [*Dickson and Brown*, 1994]. A–A' shows location of section. (b) Schematic section across Greenland-Scotland Ridge redrawn from [*Miller and Tucholke*, 1983; *Wright and Miller*, 1996]. Depths given for major spill-points of NCW over GSR.

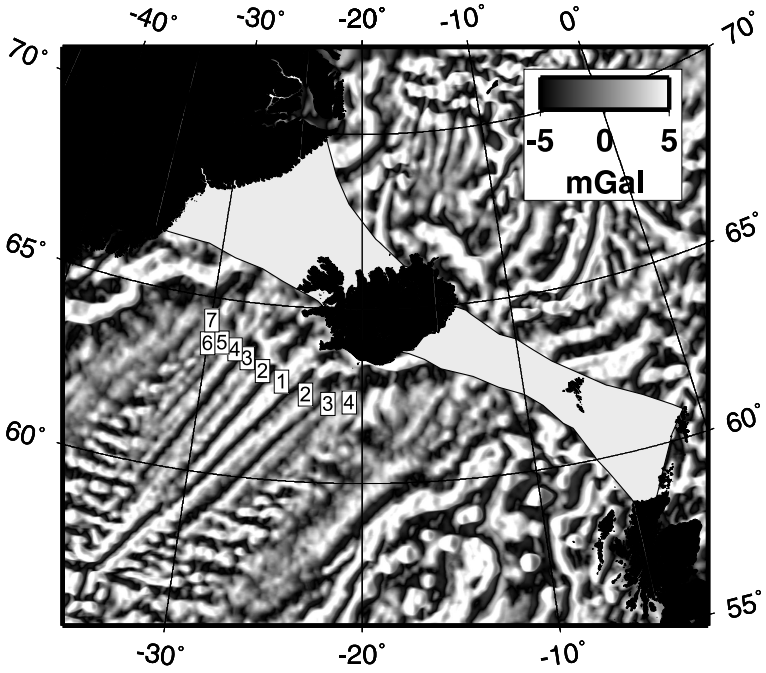


**Figure 2.** Residual free-air gravity map of North Atlantic Ocean after *Jones et al.* [2002b]. Grey lozenge = approximate location of Greenland-Scotland Ridge; numbered boxes = identified V-shaped ridges referred to in text and in Figure 10.

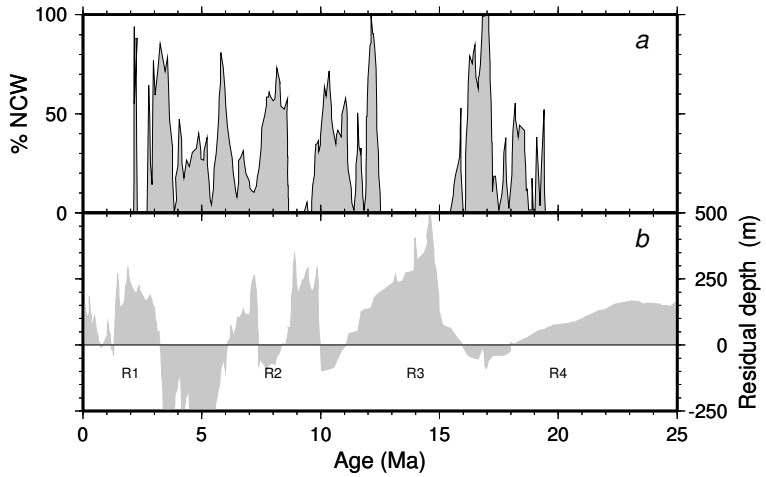


**Figure 3.** (a) Percentage overflow of Northern Component Water (%NCW); (b) residual depth data. Both taken from *Wright and Miller* [1996]. Note negative correlation between %NCW in the Southern Ocean through time and residual depth of oceanic crust at Iceland.

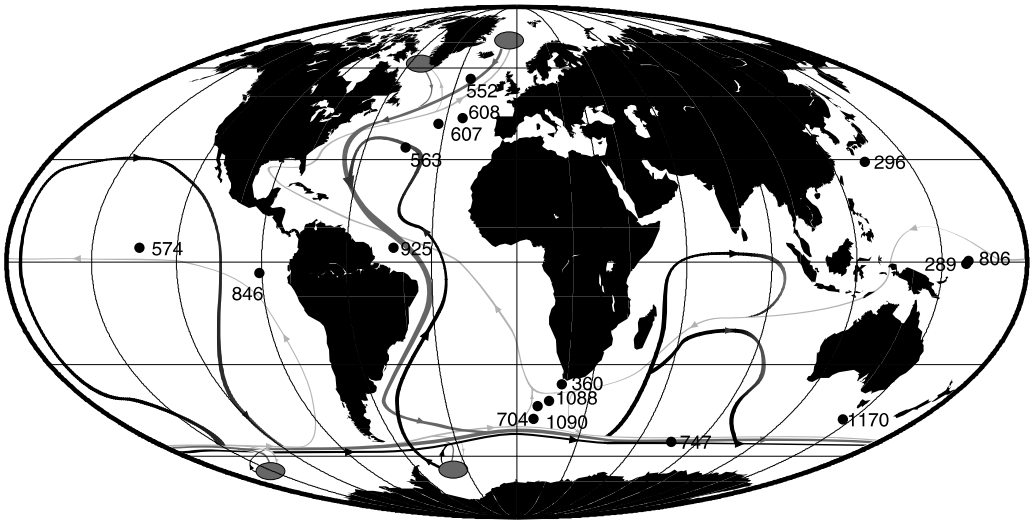


**Figure 4.** Map showing thermohaline conveyor belt [*Rahmstorf*, 2002]. Solid black lines = transport pathways of bottom water; dark grey lines = transport pathways of cold, deep water; light grey lines = transport pathways of warm, surface water; ellipses = locations of major downwelling zones; solid black circles = sites of DSDP and ODP cores used in this study.

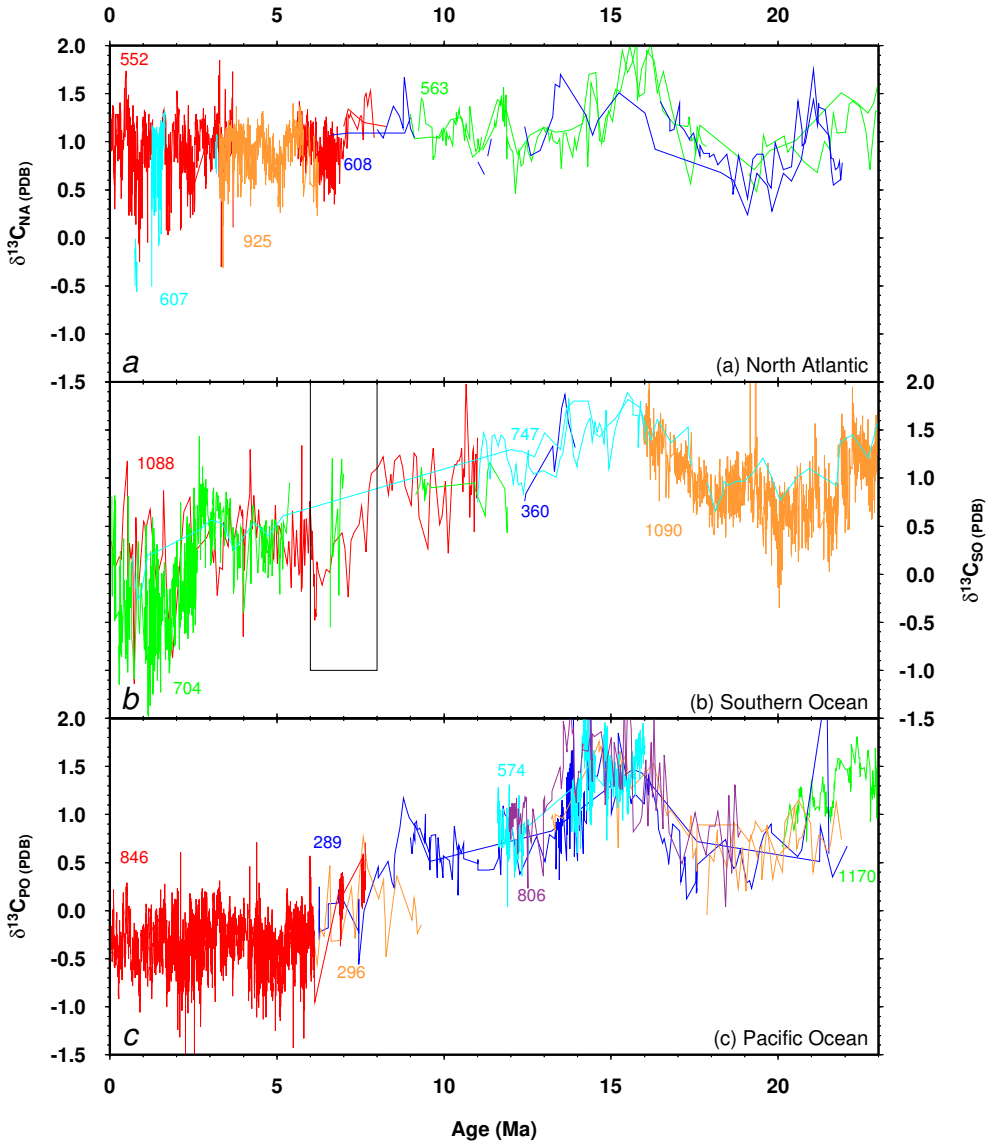


**Figure 5.** Assemblage of $\delta^{13}$C isotopic records determined from benthic foraminifera. (a) North Atlantic Ocean; (b) Southern Ocean; and (c) Pacific Ocean. Each record is colour-coded according to site (see Tables 1–3 for further details). Box shows location of Figure 14.

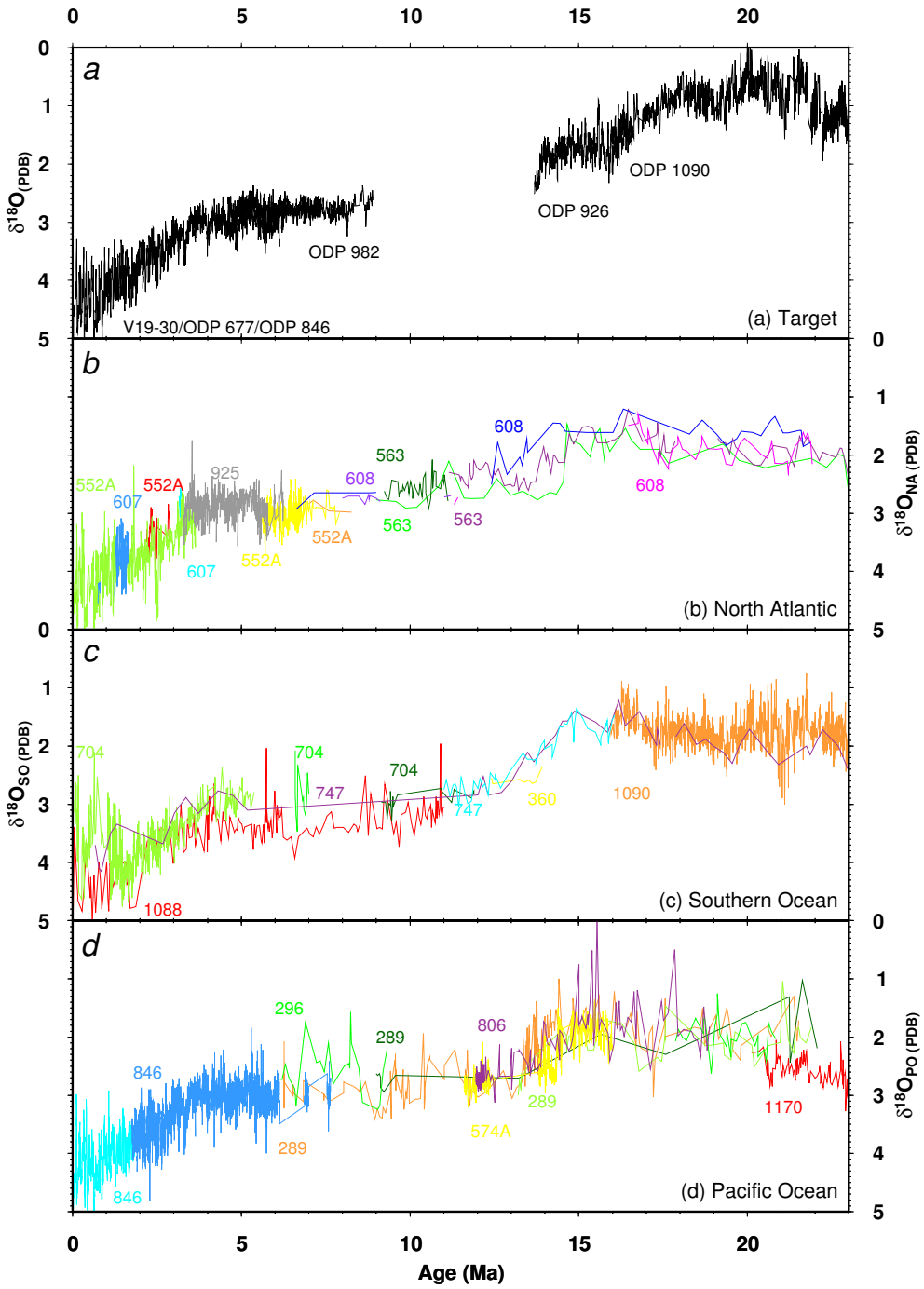


**Figure 6.** Assemblage of $\delta^{18}$O records determined from benthic foraminifera. (a) Records used as reference model; (b), (c) and (d) records from North Atlantic, Southern and Pacific Oceans, respectively, which were used to refine age models.

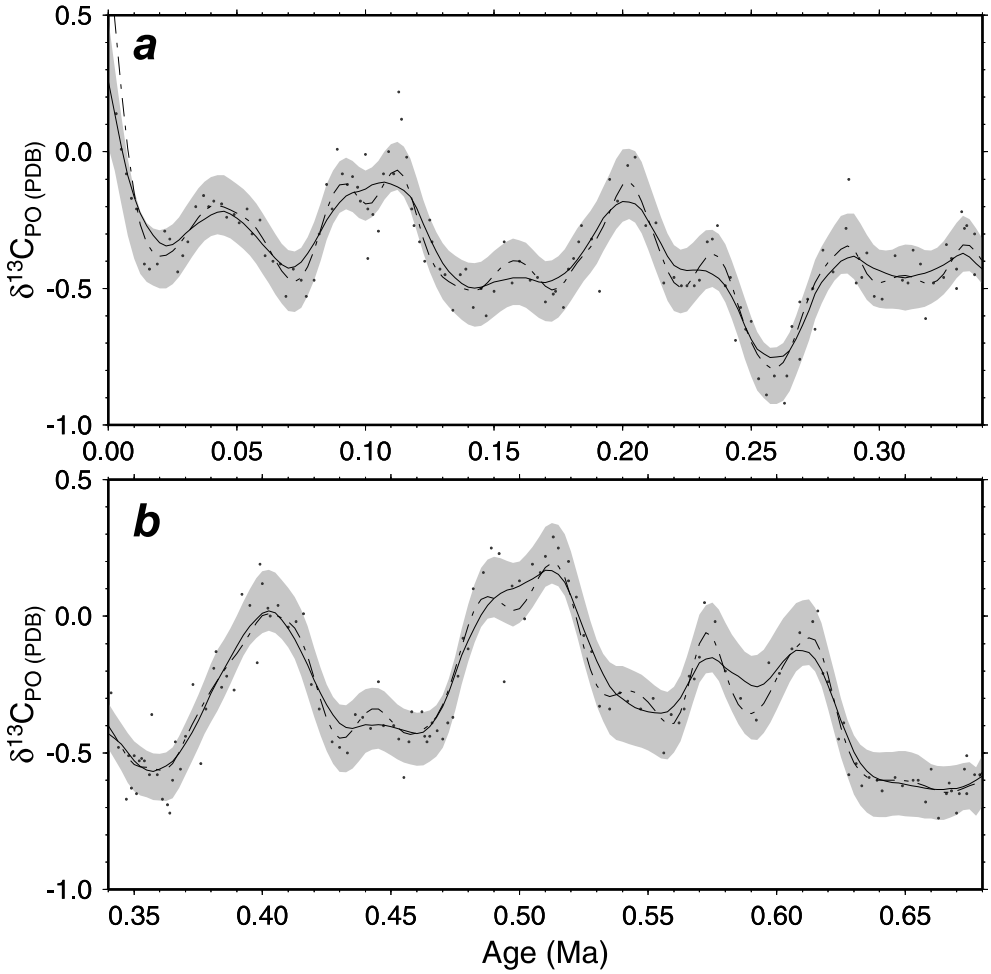


**Figure 7.** Analysis of effect of allowing for uncertainties in age determinations using 0–0.68 Ma portion of Pacific Ocean data. Solid circles = observed values; solid curve = regression estimate; dashed curve = regression estimate generated by SIMEX algorithm which removes effect of uncertainty in observed age; grey band = 95% confidence interval for standard regression estimate. Effect of SIMEX procedure is to sharpen peaks and troughs which are broadened and reduced in amplitude if observations are poorly correlated due to dating errors. Therefore, age errors do not affect the general shape of the curve (or of the resulting estimate of %NCW), but will affect the size of glacial-interglacial changes in $\delta^{13}$C and %NCW.

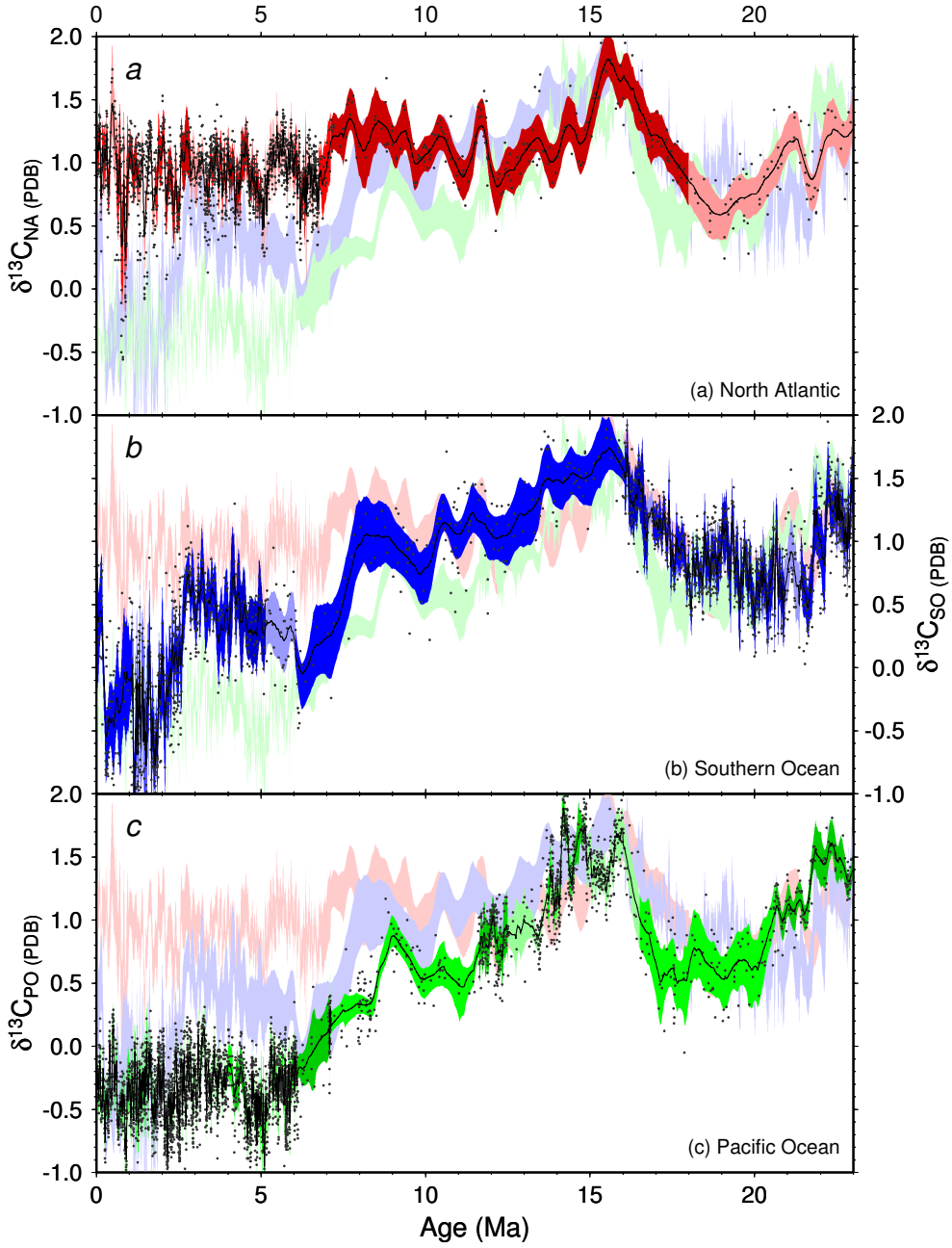


**Figure 8.** Regression estimates for three sets of composite records. In each case, other two regression estimates are shown in pale shading for comparison. (a) North Atlantic Ocean. Solid black circles = observations; solid black curve = regression estimate; bands of different red shades = 95% confidence bands for each block of data. (b) Southern Ocean. As above with green shades. (c) Pacific Ocean. As above with different blue shades. Note overlap in confidence bands between 23 and 12 Ma.

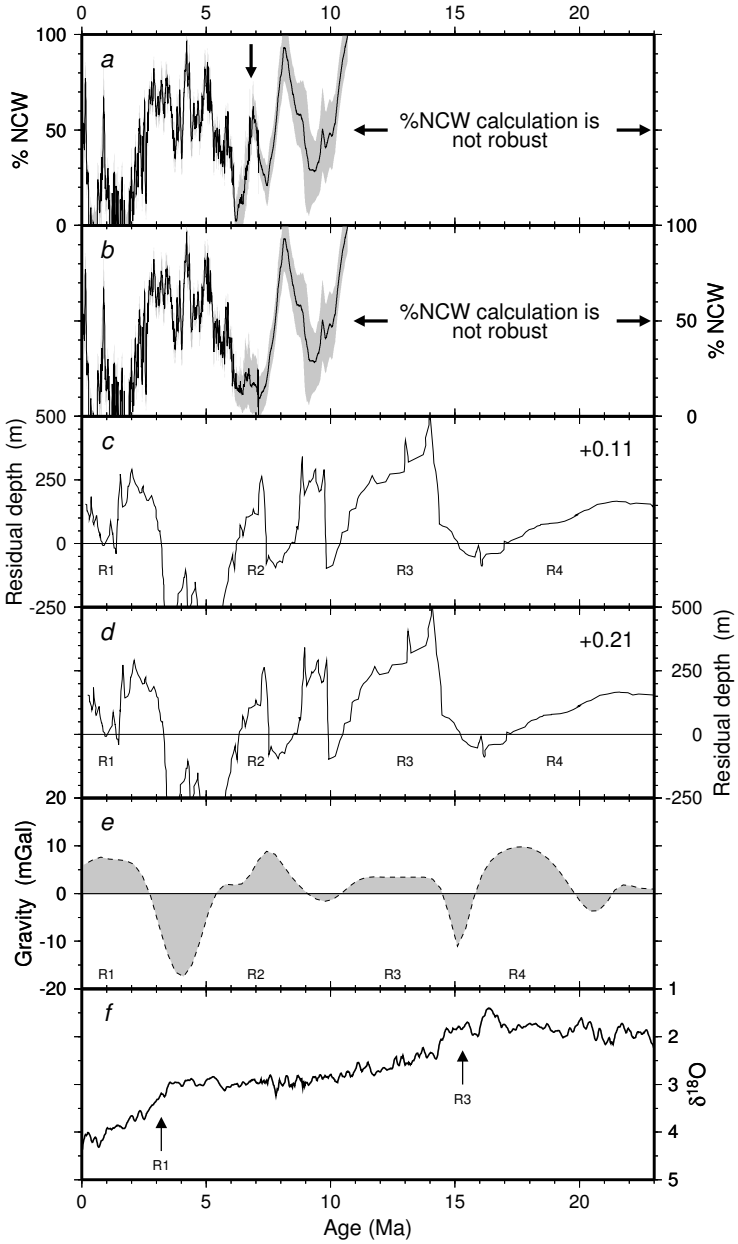


**Figure 9.** (a) Calculated %NCW record for Neogene period using data from *Müller et al.* [1991]. See Section 6.3 for a discussion of this data. Solid line = calculated variation in %NCW; grey shading = $\pm$ 1$\sigma$. (b) %NCW record with no *Müller et al.* [1991] dataset, see Tables 1–3. (c) Residual depth variation taken from *Wright and Miller* [1996] and shifted by +0.11 Ma to give best negative correlation to the %NCW record in (b). (d) Residual depth record shifted by +0.21 Ma to represent largest shift possible to represent plume-anomalies positioned beneath Denmark Straits. A time-varying correction might be more appropriate but cannot be fully justified at present. (e) Long wavelength gravity anomalies from Irminger Basin shifted for the Denmark Straits. (f) Long-term variation of global $\delta^{18}$O based on local linear regression of oxygen data from all datasets used here (Tables 1–3).

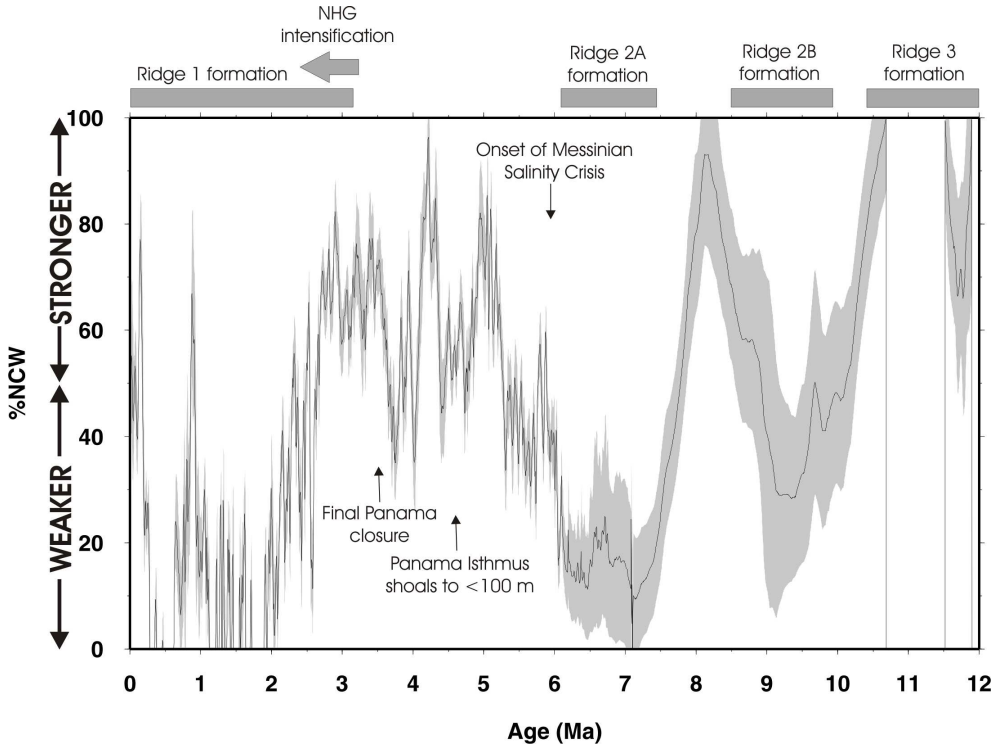


**Figure 10.** Expanded portion of Figure 10 showing %NCW for 0-12 Ma interval. Black line = calculated %NCW; grey band = $\pm$ 1$\sigma$. N.B. although calculated %NCW decreases close to zero, it is preferable to think of %NCW fluctuating from 'stronger' to 'weaker'.

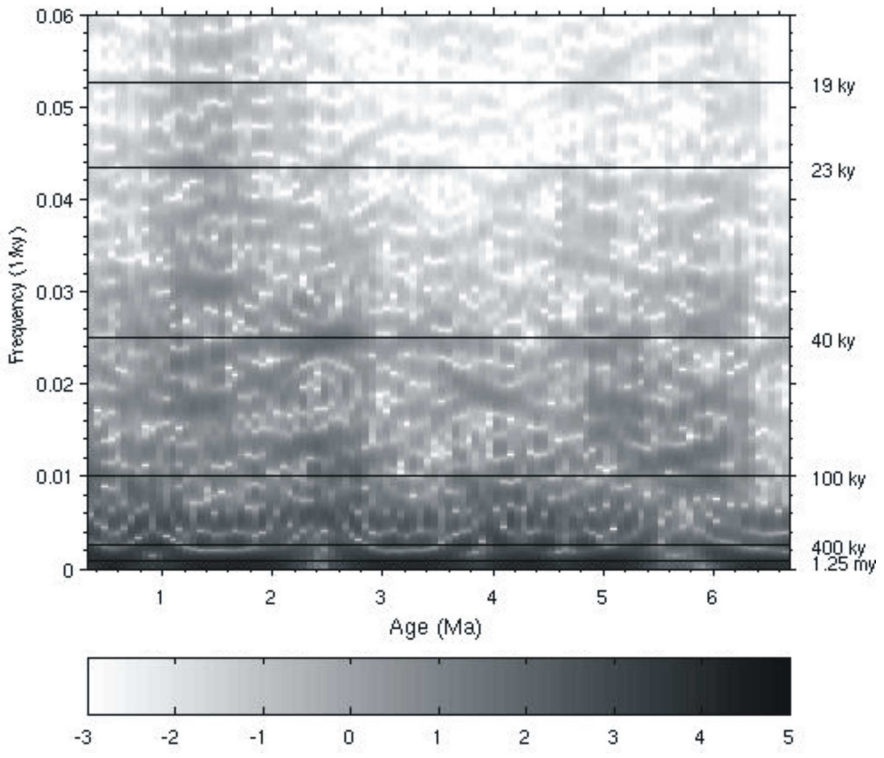


**Figure 11.** Thompson multitaper analysis of %NCW record for 0-7 Ma. Record shows persistent obliquity (i.e. 40 ka) influence whereas eccentricity (100 ka) signal is patchy between 6.1 and 5.5 Ma but more persistent from 2.8 Ma. Precessional signals are clearly evident between 1.8 and 0.8 Ma.

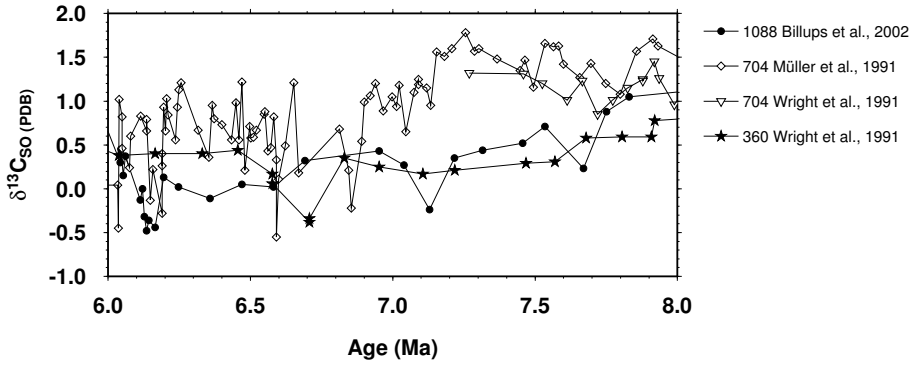


**Figure 12.** Detail of Southern Ocean $\delta^{13}$C composite record which is highlighted in Figure 5b. This portion of data generates a peak in %NCW at about 7 Ma which does not agree with activity of Iceland Plume. Close inspection reveal that ODP 704 data are shifting average values of $\delta^{13}$C upwards. If these data are removed, 7 Ma peak in %NCW disappears.

**Table 1.** Sources of Data Used in North Atlantic $\delta^{13}$C End-Member

| Site | Isotope Source | Age Model Source | Interval (Ma) | No. Points |
|---|---|---|---|---|
| 552A | *Shackleton and Hall* [1984] | *Shackleton and Hall* [1984] | 0–3.446 | 604 |
| | *Keigwin et al.* [1986] | | 5.617–8.845 | 418 |
| | *Curry and Miller* [1989] | *Curry and Miller* [1989] | 2.203–2.519 | 36 |
| | | | 2.810–2.872 | |
| | *Keigwin* [1984] | *Shackleton and Hall* [1984] | 7–8.271 | 4 |
| | | *Keigwin et al.* [1986] | | |
| 563 | *Miller and Fairbanks* [1985] | *Miller and Fairbanks* [1985] | 8.995–27.965 | 59 |
| | *Wright et al.* [1991] | *Miller and Fairbanks* [1985] | 9.223–11.121 | 39 |
| | *Wright et al.* [1992] | *Miller and Fairbanks* [1985] | 11.154–23.377 | 97 |
| 607 | *Ruddiman et al.* [1989] | *Ruddiman et al.* [1989] | 0.4–0.451 | 119 |
| | | *Clement and Robinson* [1986] | 0.522–0.567 | |
| | | | 0.750–0.810 | |
| | | | 1.251–1.648 | |
| | *Raymo et al.* [1992] | *Clement and Robinson* [1986] | 3.152–3.200 | 16 |
| 608 | *Wright et al.* [1991] | *Clement and Robinson* [1986] | 7.994–9.113 | 11 |
| | | *Miller et al.* [1991] | 11.020–11.210 | |
| | *Wright et al.* [1992] | *Clement and Robinson* [1986] | 11.301–11.422 | 48 |
| | | *Miller et al.* [1991] | 16.466–21.915 | |
| | *Miller et al.* [1987] | *Clement and Robinson* [1986] | 6.618–9.000 | 32 |
| | | | 12.414–21.872 | |
| 925 | *Billups et al.* [1997] | *Shackleton and Crowhurst* [1997] | 3.281–6.240 | 339 |
| | *Pfuhl (unpub.)* | *Tiedemann and Franz* [1997] | 3.281–6.240 | 93 |
| | *Pfuhl and Shackleton* [2004] | | 5.0-6.240 | 259 |

**Table 2.** Sources of Data Used in Southern Ocean $\delta^{13}$C End-Member

| Site | Isotope Source | Age Model Source | Interval (Ma) | No. Points |
|---|---|---|---|---|
| 360 | *Wright et al.* [1992] | *Jenkins* [1978] | 12.413–13.922 | 9 |
| 704 | *Hodell and Ciesielski* [1991] | *Hailwood and Clement* [1991] | 0.056–5.377 | 642 |
| | | *Hodell and Ciesielski* [1991] | | |
| | *Wright et al.* [1991] | *Hailwood and Clement* [1991] | 9.155–9.632 | 17 |
| | | | 10.920–11.890 | |
| 747 | *Wright and Miller* [1992] | *Heider et al.* [1992] | 11.005–16.065 | 57 |
| | | *Berggren* [1992] | 24.12–26.37 | |
| | Billups unpub. data | As above | 0.667–25.374 | 27 |
| 1088 | *Billups* [2002] | *Shipboard Scientific Party* [1999] | 0–11.004 | 158 |
| 1090 | *Billups et al.* [2004] | *Billups et al.* [2004] | 15.94–24.19 | 1532 |

**Table 3.** Sources of Data Used in Pacific Ocean $\delta^{13}$C End-Member

| Site | Isotope Source | Age Model Source | Interval (Ma) | No. Points |
|---|---|---|---|---|
| 289 | *Savin et al.* [1981] | *Srinivasan and Kennett* [1981] | 4.797–21.521 | 220 |
| | *Woodruff and Savin* [1989] | *Shipboard Scientific Party* [1975] | 5.538–22.060 | 12 |
| | *Woodruff and Savin* [1991] | | 13.203–21.896 | 42 |
| 296 | *Savin et al.* [1981] | *Ellis* [1975] | 6.099–11.454 | 16 |
| | | | 17.864–20.834 | 30 |
| 574A | *Pisias et al.* [1985] | *Gartner and Chow* [1985] | 11.604–16.012 | 495 |
| 806 | *Corfield and Cartlidge* [1993] | *Takayama* [1993] | 11.951–18.881 | 126 |
| 846 | *Mix and Shackleton* [1995] | *Shackleton et al.* [1995a] | 0–1.849 | 697 |
| 846 | *Shackleton et al.* [1995b] | *Shackleton et al.* [1995a] | 1.763–7.644 | 2314 |
| 1170 | *Pfuhl and McCave* [2004] | *Pfuhl and McCave* [2004] | 20.119–28.112 | 269 |